Clim. Past Discuss., 11, 4159–4204, 2015
www.clim-past-discuss.net/11/4159/2015/
doi:10.5194/cpd-11-4159-2015

Climate of the Past Discussions
Open Access

The Paleoclimate reanalysis project

S. A. Browning and I. D. Goodwin

Marine Climate Risk Group, Department of Environmental Sciences, Macquarie University, North Ryde, Australia

Received: 11 August 2015 – Accepted: 12 August 2015 – Published: 1 September 2015

Correspondence to: S. A. Browning (stuart.browning@mq.edu.au)

Published by Copernicus Publications on behalf of the European Geosciences Union.

Abstract

Recent advances in proxy-model data assimilation have made feasible the development of proxy-based reanalyses. Proxy-based reanalyses aim to make optimum use of both proxy and model data while presenting paleoclimate information in an accessible format – they will undoubtedly play a pivotal role in the future of paleoclimate research. In the Paleoclimate Reanalysis Project (PaleoR) we use "off-line" data assimilation to constrain the CESM1 (CAM5) Last Millennial Ensemble (LME) simulation with a globally distributed multivariate proxy dataset, producing a decadal resolution reanalysis of the past millennium. Discrete time periods are "reconstructed" by using anomalous ($\pm 0.5\sigma$) proxy climate signals to select an ensemble of climate state analogues from the LME. Prior to assimilation the LME simulates internal variability that is temporally inconsistent with information from the proxy archive. After assimilation the LME is highly correlated to almost all included proxy data, and dynamical relationships between modelled variables are preserved; thus providing a "real-world" view of climate system evolution during the past millennium. Unlike traditional regression based approaches to paleoclimatology, PaleoR is unaffected by temporal variations in teleconnection patterns. Indices representing major modes of global ocean–atmosphere climate variability can be calculated directly from PaleoR spatial fields. PaleoR derived ENSO, SAM, and NAO indices are consistent with observations and published multiproxy reconstructions. The computational efficiency of "off-line" data assimilation allows easy incorporation and evaluation of new proxy data, and experimentation with different setups and model simulations. PaleoR spatial fields can be viewed online at http://climatefutures.mq.edu.au/research/themes/marine/paleor/.

CPD
11, 4159–4204, 2015

1 Introduction

Reanalyses combine meteorological observations and numerical model simulations to produce a realistic estimate of the state of the system, in recent decades they have revolutionised the way in which weather and climate research are conducted (e.g. Dee et al., 2011; Kalnay et al., 1996). Extending reanalyses back in time has been a major research focus (e.g. Compo et al., 2011). However, observational data scarcity prior to the 20th century is the limiting factor. Without the benefit of "real-world" data, model simulations of past climate cannot be expected to match the temporal evolution of the climate system (Bengtsson et al., 2006). Therefore, efforts to understand "real-world" climate variability over longer timescales must rely on climate signals preserved in proxy records such as ice cores and tree rings. A paleoclimate reanalysis could potentially make optimum use of proxy and model data while presenting paleoclimate information in an accessible format suitable for a wide range of research applications.

However, extracting coherent climatic signals from spatially dispersed multiproxy data is a non-trivial exercise plagued by high uncertainties and methodological challenges (Ammann and Wahl, 2007; Jones et al., 2009; Mann et al., 2005; Smerdon et al., 2013). For example, traditional approaches that look for a common signal amongst multiple proxy records are often based on the false assumption that covariance relationships remain stable through time (Gallant et al., 2013; Li and Smerdon, 2012); they also have difficulty incorporating data representing multiple climatic variables and seasonal sensitivities. Furthermore, variational assimilation schemes used in meteorological reanalysis, such as NCEP1 and ERA-Interim, are unsuitable for sparse low-resolution paleoclimate data (Widmann et al., 2010). Nevertheless, recent advances in proxy-specific data assimilation techniques have addressed many of these issues (Bhend et al., 2012; Franke et al., 2010; Goodwin et al., 2013, 2014; Goosse et al., 2006; Graham et al., 2007; Hakim et al., 2013; Schenk and Zorita, 2012; Steiger et al., 2013; Widmann et al., 2010) and made feasible the development of proxy based climate reanalysis.

CPD
11, 4159–4204, 2015

Proxy data assimilation can occur at model runtime (on-line) or can be applied to existing model simulations (off-line). One of the major constraints associated with "on-line" assimilation is the high computational cost of running millennial length or longer simulations, leading to the use of simplified models (e.g. Goosse et al., 2010). It has been shown that in many situations runtime assimilation is not really necessary or advantageous (Bhend et al., 2012). "Off-line" proxy data assimilation significantly reduces computational demands and provides the opportunity to utilize existing high-resolution climate model simulations (Steiger et al., 2013).

This article describes our efforts at developing a globally relevant paleoclimate reanalysis (hereafter referred to as PaleoR) of the past 1200 years at decadal resolution. We employ the "off-line" data assimilation scheme described in Goodwin et al. (2013, 2014) where it was used to investigate atmospheric circulation patterns during the Medieval Climate Anomaly. Whereas Goodwin et al. (2013, 2014) used only Southern Hemisphere proxy data and a 10 000 year unforced simulation from the low resolution CSIRO Mk3l model, this paper employs a globally distributed multivariate proxy dataset and the recently released CESM1 (CAM5) Last Millennial Ensemble simulation (Otto-Bliesner et al., 2015). The paper is structured as follows: Sect. 2 describes the proxy dataset, model data and the assimilation scheme; Sect. 3 evaluates PaleoR using 3 complementary approaches; Sect. 4 discusses advantages, limitations and planned improvements to PaleoR; and Sect. 5 provides some concluding remarks.

2 Methods

The multivariate data assimilation (MDA) approach used to develop PaleoR is described below and in Goodwin et al. (2013, 2014) and Browning (2014). MDA reconstructs discrete time periods by using information from a multivariate suite of proxy data to select climate state analogues from an existing AOGCM simulation.

CPD
11, 4159–4204, 2015

2.1 Proxy dataset

The multivariate proxy dataset includes individual proxy records, published reconstructions, and regional multiproxy reconstructions (Fig. 1 and Table A1). Proxy screening as applied in many paleoclimate reconstructions (e.g. Cook et al., 1999) is not required for MDA as there is no prerequisite for covariability. Proxy data of varying temporal resolutions are accommodated, including records representing discrete time periods; Fig. 1b shows the mean temporal resolution of all included proxy data at each timestep. Most proxy records contain a component of chronological uncertainty that increases back in time; this is partially reflected by a corresponding decrease in temporal resolution (Fig. 1b). In recognition of this uncertainty PaleoR is currently executed at decadal resolution. For each discrete decadal time period proxy climatic signals are calculated using 10 year means post 1400 AD and running 20 year means prior to 1400 AD. To facilitate the inter-comparison of proxy data representing different variables, all decadal data are normalized relative to the 1300–2000 AD long-term mean. Most proxy records contain a component of non-climatic "noise" resulting a relatively high signal-to-noise ratio when compared with observational data. To account for this, each decade is reconstructed independently, using only proxies displaying an unambiguous climatic signal: defined as the decadal mean exceeding $\pm 0.5\sigma$. Figure 1b shows the number of proxy records included in the assimilation each time step. The normalized values for each retained proxy are combined into a vector ($\boldsymbol{P}$) for each time period.

2.2 Model dataset

The model dataset used for PaleoR is the CESM1 (CAM5) Last Millennium Ensemble (Otto-Bliesner et al., 2015), hereafter referred to as LME. LME uses a $\sim 2^{\circ}$ atmosphere and $\sim 1^{\circ}$ ocean and sea ice version of CESM1-CAM5. The LME consists of 10×1156 year simulations spanning 850 to 2005 AD. All simulations are forced with reconstructions of solar intensity, volcanic emissions greenhouse gasses, aerosols, land use conditions and orbital parameters. For additional details on the LME setup and

CPD
11, 4159–4204, 2015

evaluation see Otto-Bliesner et al. (2015). Prior to assimilation both model and proxy data must be in a comparable format. Therefore, in the assimilation algorithm model data are represented by an array of normalized annual mean timeseries (S) derived from the same locations and from the equivalent modelled climate variables as the proxy records in $\boldsymbol{P}$. All proxy data are calibrated to modelled temperature, precipitation, sea surface temperature (SST), or sea-level pressure (SLP) based on previously published interpretations (Table A1). To account for seasonality, annual means are calculated from the seasons of proxy sensitivity.

2.3 Assimilation

The MDA approach reconstructs discrete time periods by searching the model data for climate state analogous to the combined signal from all included proxy data (Goodwin et al., 2013, 2014). Each year of the LME represents an individual multivariate realization of a physically plausible climate state. In this respect the interannual temporal continuity of the LME can be discarded, thereby giving an effective ensemble size of 11 560 members. Individual ensemble members analogous to the proxy inferred climate states for each time period are identified by calculating the Euclidean distance between the normalized proxy data ($\boldsymbol{P}$) and the normalized model data (S_{1-n}) as described by Eq. (1):

$$D_n = \sum |\boldsymbol{P}_i - S_{ni}| \quad (1)$$

$\boldsymbol{P}$ is a vector (width = i) of normalized proxy values, where each element represents the climatic signal (temperature, precipitation, SST, or SLP) from a single proxy record or reconstruction during the designated time period. S is an array of timeseries (length = n, width = i) derived from the LME at the equivalent locations and climate variables as the elements of $\boldsymbol{P}$. Each column of S_{1-i} corresponds to each element of $\boldsymbol{P}_{1-i}$, and each row of S_{1-n} represents one year (ensemble member) of the LME. D_n is the Euclidean distance between $\boldsymbol{P}$ and each ensemble member (n), where $D_n = 0$ would indicate

CPD
11, 4159–4204, 2015

a perfect match. D_{1-n} is a measure of the total difference between all elements of $\boldsymbol{P}$ and S_{1-n}. Therefore, the minima of D_{1-n} represent ensemble members that are the best matching analogues (BMA) for the climate state described by the multivariate proxy dataset ($\boldsymbol{P}$) and are used to define each time period.

In numerical weather forecasting it is common practice to take an ensemble mean and use the ensemble spread to estimate uncertainty: where the ensemble spread is large, uncertainty is increased. This is also the case in the development of re-analysis products such as the 20th Century Reanalysis (20CR), where the climate state is defined by the mean of a 56-member ensemble and uncertainty is estimated from the ensemble spread (Compo et al., 2011). A similar approach is also adopted for PaleoR, where the reconstructed climate state is defined by the ensemble mean of the 50 BMA and ensemble spread provides one estimate of uncertainty. Using 50 BMA is found to provide the optimal balance between including contributions from the maximum number of proxy records while minimizing the mean Euclidean distance. 50 BMA also provides a large enough sample size to calculate statistical significance (Browning, 2014; Goodwin et al., 2013).

Modelled climate variables can be resolved by compositing the 50-BMA ensemble; as all modelled variables are dynamically consistent, theoretically any modelled variables can be calculated. However, at present we are utilizing only variables with a mechanistic relationship to the multiproxy dataset: air temperature, precipitation, SST, SLP, and winds. Anomalies are calculated relative to the full LME and therefore represent deviations from the modelled past millennial climate, not the observed modern climate.

2.4 Evaluation

We evaluate the skill of the MDA using 3 complementary approaches: (1) comparison with the included proxy data; (2) pseudoproxy based "reconstruction" of a known climate; and (3) calculation of major modes of global climate variability and comparison with equivalent previously published multiproxy reconstructions.

CPD
11, 4159–4204, 2015

2.4.1 Comparison with proxy data

The first evaluation tests the skill of MDA in creating a climate dataset that is consistent with the included proxy data. This can be tested by directly comparing PaleoR with the multiproxy dataset; PaleoR should also show a considerable improvement when compared to a transient simulation of the same time period without data assimilation. The experimental setup is relatively straightforward and consistent with a similar comparison performed by Goosse et al. (2006). An array of synthetic proxy records are extracted from PaleoR – at the same locations and from the equivalent climate variables as the proxy records – and compared with the original proxy records (decadally averaged). To compare against the null-case, of no data assimilation, the proxy records are also compared to the LME (mean of the 10 ensemble members) without data assimilation.

2.4.2 Pseudoproxy evaluation

The second evaluation tests the skill of MDA in reconstructing global patterns of variability given the spatial distribution of the proxy dataset. This test uses pseudoproxy data to evaluate the skill of MDA at reconstructing the known climate of a model simulation using a synthetic proxy network (Jones et al., 2009; Mann et al., 2007). The known climate is a single ensemble member of the LME: LME^{01}. Pseudo proxies are derived from LME^{01} using the same locations and equivalent variables as the proxy network listed in Table A1. A signal to noise ratio of 0.33 is added to each pseudo proxy to simulate real-world uncertainty (Bhend et al., 2012). The 1156 year LME^{01} simulation is then "reconstructed" at 10 year resolution using the MDA approach to select climate state analogues from the remaining 9 LME members, based only on the climate signals from the pseudoproxy network – effectively producing a pseudoproxy based PaleoR ($PaleoR^{pseudoproxy}$). Grid point correlations (Pearson's r) for selected variables are then used to evaluate the similarity between LME^{01} and $PaleoR^{pseudoproxy}$.

CPD
11, 4159–4204, 2015

2.4.3 Comparison with existing multiproxy reconstructions

The third evaluation examines PaleoR as a tool for investigating multiple large-scale components of the climate system. Indices representing the major modes of global climate variability: El Niño Southern Oscillation (ENSO), Southern Annular Mode (SAM), and the North Atlantic Oscillation (NAO) are calculated directly from PaleoR spatial fields in much the same way as they are typically calculated from model or reanalysis data. Each index is compared to previously published multiproxy reconstructions and equivalent indices calculated from observational-based data. As PaleoR is at decadal resolution, robust comparisons with observational records are difficult due to the limited temporal overlap and reduced degrees of freedom associated with decadally averaged data.

ENSO is the leading coupled ocean–atmosphere mode of global climate variability (e.g. Trenberth et al., 2005). A PaleoR ENSO index is calculated from SSTa in the Niño 3.4 region (after Trenberth, 1997) and compared with two recent multiproxy ENSO reconstructions (Emile-Geay et al., 2013b; McGregor et al., 2010) and an equivalent index derived from HadISST (1870–2012). During the late 20th century SAM has been the leading mode of atmospheric variability (Trenberth et al., 2005). A PaleoR SAM index is calculated as the leading Empirical Orthogonal Function (EOF) of Southern Hemisphere sea-level pressure between 20 to 82° S using the approach of (Visbeck and Hall, 2004), and compared with two recent multiproxy reconstructions (Abram et al., 2014; Villalba et al., 2012) and an equivalent SAM index calculated from the 20CR (1871–2012). However, it must be stressed that there is considerable uncertainty as to the state of the SAM prior to ∼ 1950 due to lack of observational data (Ho et al., 2011). The NAO is the dominant mode of atmospheric variability in the North Atlantic region (Hurrell, 1995). A PaleoR NAO index is calculated as the leading EOF of Northern Hemisphere sea-level pressure between 20 to 80° N and 90° W to 40° E (after Hurrell, 1995), and is compared with two recent multiproxy reconstructions (Ortega et al., 2015; Trouet et al., 2009) and the published NCAR EOF based NAO index

CPD
11, 4159–4204, 2015

(NCAR 2015). In each case the climate indices are first calculated from the unassimilated LME. Index values for each time period are then calculated from the mean of the 50-BMA, the ensemble spread providing one estimate of uncertainty.

3 Results

3.1 Comparison with proxy data

Figure 2a shows strong agreement between PaleoR and the proxy archive, with correlations exceeding 99 % significance at most locations. However, there are some records and some time periods that do not agree. In these situations the climate signal from the proxy in question, when evaluated against all other proxies, contains a signal that is not consistent with any of the modelled climate states. This can occur because of either errors in proxy dating or climatic interpretation, or the LME dataset does not contain a complete sample of all past millennium regional climate states. Comparison between the unassimilated LME ensemble mean and the proxy archive shows reasonably good correspondence, however only a few correlations exceed 99 % significance (Fig. 2b) – similar results are observed when individual LME ensemble members are used. The mean correlation value (absolute r) calculated across all proxy records for PaleoR is $r = 0.6$ ($n = 115$, $p = 0.03$) compared with $r = 0.19$ ($n = 115$, $p = 0.3$) for the unassimilated LME ensemble mean. LME provides a realistic simulation of internal climate variability that is temporally inconsistent with most proxy evidence. By incorporating proxy data using MDA, PaleoR presents a more realistic evolution of climate system internal variability – as defined by proxy data – than does the unassimilated LME.

3.2 Pseudoproxy experiment

Figure 3 shows grid point correlations between $\text{PaleoR}^{\text{pseudoproxy}}$ and LME^{01} SLP, air temperature, SST, and precipitation over 1156 model years at 10 year resolution; it provides an indication of the skill of the MDA approach when applied to the LME, given

CPD
11, 4159–4204, 2015

the available proxy data network (Fig. 1; Table A1). PaleoR spatial fields, based on real proxy data, should be interpreted with most confidence in the regions indicated by significant positive correlations ($r > 0.25$, $p < 0.01$, $n = 115$; indicated by stippling in Fig. 3). PaleoR^{pseudoproxy} skill appears to be closely related to proxy data availability. Overall performance is best in regions with the highest density of proxy data, such as the Pacific Northwest, Western Europe, Australia-New Zealand and the South America-Antarctic Peninsular sectors.

PaleoR^{pseudoproxy} successfully reconstructs SLP over the Antarctic (regional mean $r = 0.59$) and most of the Southern Hemisphere mid-latitudes (regional mean $r = 0.43$) giving confidence to the PaleoR based SAM index. Confidence is lower in the Northern Hemisphere, with lower correlation values over central North America (regional mean $r = 0.27$) and Eurasia (regional mean $r = 0.26$) where proxy data density is limited. Correlation values are slightly higher over the North Atlantic region (regional mean $r = 0.4$), where there is a greater density of proxy data, giving some confidence to the PaleoR NAO index presented in Sect 2.5.3. Air temperature is well reconstructed over most areas with a global mean of $r = 0.46$. SST fields appear to be well reconstructed in the Pacific (regional mean $r = 0.56$), Indian (regional mean $r = 0.48$) and Atlantic (regional mean $r = 0.51$) ocean basins. Strong SST correlations in the central Pacific give confidence to the PaleoR based Niño 3.4 SST index. Precipitation fields show the least confidence (global mean $r = 0.25$) and appear to be only valid close to the proxy locations, possibly due to way in which localised precipitation is represented in the model.

Direct translation of the pseudoproxy experiment results into uncertainty estimates for PaleoR is not straightforward, however they do provide a valuable framework for methodological refinement and qualitative interpretation. Because of this, quantitative error estimates are based on the 50-BMA-ensemble spread, similar to the approach used in weather forecasting and observational reanalyses. The pseudoproxy experiment results should therefore be viewed as a qualitative supplement to the ensemble spread when assessing PaleoR confidence.

CPD
11, 4159–4204, 2015

3.3 Climate index comparison

The objective of this section is to demonstrate that PaleoR can be used to investigate behaviour in the primarily global modes of atmosphere–ocean variability and provides an alternative to traditional paleoclimate methods that look for a common signal amongst multiple proxy records. PaleoR derived indices of Niño 3.4 SST, SAM and NAO are compared to equivalent indices developed using traditional approaches. All of the comparison indices were constructed by finding a common signal amongst multiple records that is statistically correlated to the target index over the observational period. As part of this process, proxy records that do not co-vary over the length of the reconstruction are discarded. For example Ortega et al. (2015) were forced to discard > 80 % of their initial proxy dataset due to non-covariance. This practice discards valuable information, particularly if the time periods of non-covariance represent non-canonical behaviour of the index in question. ENSO indices provide an excellent example, as there is now a large body of work devoted to understanding different "flavours" of ENSO (e.g. Ashok et al., 2007; Newman et al., 2011) and their different teleconnection responses (e.g. Graf and Zanchettin, 2012).

The PaleoR indices presented here are calculated from actual modelled SST or SLP data. Climate signals at the locations from which they are derived are linked to proxy climatic signals via the dynamic equations of state used to drive the model. As long as the LME can simulate non-canonical behaviour, PaleoR indices are unaffected by changes in teleconnection patterns. In contrast, the comparison indices are a statistical representation of covariance between multiple records that, over the calibration period are correlated to the target index. This a priori requirement for covariance ensures traditional approaches cannot resolve variability that lies outside the range of modern observations. When comparing PaleoR indices with previous work it is important to keep in mind the different methodologies. Time periods when PaleoR differs from the comparison indices are likely to represent periods of non-canonical behaviour in the major modes, which can be further investigated using PaleoR spatial fields.

CPD
11, 4159–4204, 2015

3.4 ENSO reconstructions

Figure 4a shows a moderate to strong correlation between the Niño 3.4 SST indices derived from PaleoR and HadISST ($r = 0.6$, $p = 0.02$, $n = 14$). There is also good agreement between the PaleoR Niño 3.4 and the McGregor et al. (2010) Unified ENSO Proxy (UEP) ($r = 0.6$, $p < 0.01$, $n = 33$). The UEP is derived from a common signal in several published ENSO reconstructions and is representative of Pacific decadal variability; it is not a specific SSTa reconstruction per se, but represents a general evolution of ENSO related variability as interpreted from proxies both central to Niño 3.4 and from teleconnected regions over the past 350 years. The two ENSO reconstructions do share some proxy records, however they are developed from fundamentally different approaches. Emile-Geay et al. (2013) recently published a longer Niño 3.4 reconstruction dating back to 1150 AD, including a range of proxy evidence from central Pacific and teleconnected regions. Overall the PaleoR Niño 3.4 is moderately correlated to the Emile-Geay et al. (2013) Niño 3.4 ($r = 0.42$, $p < 0.01$, $n = 85$). The two reconstructions appear to be in excellent agreement from 1150 to 1300 AD; however, they differ considerably during several more recent periods, including 1400 to 1550 AD. For example, strong El Niño signals in 1590 AD and 1840 AD are not captured in the Emile-Geay et al. (2013) Niño 3.4, whereas the 1840 AD event is prominent in both the UEP and PaleoR reconstructions. Differences are likely due to both proxy data selection and the Regularized Expectation (RegEM) method used by Emile-Geay et al. (2013a).

All three ENSO reconstructions are in general agreement, however PaloeR provides the added advantage of resolving dynamically consistent spatial patterns of coupled ocean–atmosphere variability beyond the Niño 3.4 region. Figure 5 shows an example of SST and SLP anomalies for positive and negative Niño 3.4 index periods. The spatial SST anomaly structure and extratropical atmospheric teleconnections associated with canonical ENSO are broadly consistent with observations: in the North Pacific there is a strengthening (weakening) of the Aleutian Low under El Niño (La Niña) conditions (Bjerknes, 1966, 1969; Lau, 1997); and in the South Pacific there is a weakening

CPD
11, 4159–4204, 2015

(strengthening) of the Amundsen Sea low under El Niño (La Niña) conditions (Mo and Higgins, 1998; Turner et al., 2013). This is expected, as the MDA approach preserves dynamical linkages between modelled climate variables.

3.5 Southern annual mode reconstructions

Figure 4b shows a moderate to strong correlation between SAM indices derived from PaleoR and the 20CR ($r = 0.72$, $p < 0.01$, $n = 14$). There is a moderate to strong correlation between the PaleoR SAM and the Villalba et al. (2012) SAM reconstruction ($r = 0.62$, $p < 0.01$, $n = 60$) despite being derived from different methodologies and mostly different proxy networks: although there are some individual proxies common to both. The PaleoR SAM is also moderately correlated to the longer Abram et al. (2014) SAM reconstruction ($r = 0.52$, $p < 0.01$ $n = 101$); the two indices agree on a general strengthening since 1400 AD, however they disagree during many decades prior to 1400 AD.

Both the Villalba et al. (2012) and Abram et al. (2014) SAM reconstructions are calculated from the common signal in warm season proxies. PaleoR SAM accommodates proxies sensitive to both summer and winter climate variability and is also correlated to the early winter SAM reconstruction of Goodwin et al. (2004) ($r = 0.47$, $p < 0.01$, $n = 100$). Although this relationship is expected as the Goodwin et al. (2004) SAM reconstruction is based only on the Law Dome Sea Salt record, that is included in PaleoR (Fig. 1; Table A1).

Reconstructing SAM from midlatitude proxies can be challenging, as teleconnections between SAM and some midlatitude regions can breakdown or reverse depending on the influence of the tropical pacific (Fogt and Bromwich, 2006). Traditional paleoclimate reconstruction techniques that look for a common signal amongst multiple records struggle to accommodate changing teleconnection patterns and seasonal biasa. PaleoR is unaffected by these issues, the second EOF of PaleoR SLP resembles the Pacific South America pattern (Mo and Ghil, 1987) and is highly correlated to the PaleoR Niño 3.4 index (Goodwin et al., 2013). PaleoR is therefore able to resolve tem-

CPD
11, 4159–4204, 2015

poral variations in the nature of mid to high latitude teleconnection patterns and their influence on the SAM (Goodwin et al., 2013).

3.6 North Atlantic oscillation reconstructions

Figure 4c show the PaleoR NAO is broadly consistent with the observational NCAR NAO index ($r = 0.54$, $p = 0.09$, $n = 11$). There is a moderate correlation between the PaleoR NAO the recent Ortega et al. (2015) NAO index ($r = 0.48$, $p < 0.01$, $n = 92$). However, PaleoR NAO is only weakly correlated to the Trouet et al. (2009) NAO index ($r = 0.23$, $p = 0.03$, $n = 95$). All three NAO reconstructions are in general agreement for most multidecadal periods, such as positive NAO during the early Medieval Climate Anomaly (MCA) at ~ 1150 AD and negative NAO during the early Little Ice Age at 1550 to 1600 AD. However, they differ considerably during other periods, such as the late MCA, post ~ 1250 AD, when PaleoR does not simulate a persistent positive NAO.

The NAO has strong climatic linkages with many global regions (e.g. Hurrell and Deser, 2009); therefore the state of the NAO should be consistent with proxy signals from many parts of the Northern Hemisphere. The PaleoR is highly correlated to most proxy data from the North Atlantic region so it should provide a robust estimate of past NAO behaviour, irrespective of variations in teleconnection patterns. A detailed investigation into the NAO behaviour over the past millennium is beyond the scope of this paper. However, PaleoR resolves full spatial fields that can be used to better elucidate the nature of past climatic changes; as an example, Fig. 5 shows SLP patterns for both positive and negative phases of the NAO index.

4 Discussion

PaleoR was designed first and foremost to be a paleoclimate research application; in this respect we did not design the PaleoR as a static dataset, rather as experimental tool that can be easily tailored to specific research objectives. This section discusses

CPD
11, 4159–4204, 2015

some of the advantages and limitations of the current PaleoR version. We also identify several areas where modifications to the current approach might be expected yield improvements in future versions.

4.1 Advantages

PaleoR is developed using a relatively simple MDA approach that is computationally efficient and can be readily applied to existing model simulations. To-date we have experimented with simulations from Mk3L (Goodwin et al., 2013, 2014), CM21, CCSM4, GISS, HadCM3 and MIROC-ESM. Unfortunately most of the CMIP5 past millennium simulations contain too few ensemble members to provide a large enough ensemble for analogue selection. LME was chosen for this version due to the high resolution, realistic forcing and large available ensemble. After initial setup, a 1000 year reanalysis at decadal resolution without figure production can be calculated in less than one minute on a standard laptop computer. The minimal computation demands of "off-line" verses "on-line" data assimilation allow easy experimentation with various setups. The proxy dataset is organized as recommended by Emile-Geay and Elsham (2013) allowing easy modification of included proxy data and easy inclusion of new records as they become available. The assimilation can also be run at varying temporal resolutions in order to take full advantage of proxy chronological confidence without running the risk of over-interpretation.

As a tool for researching long term climate variability, data assimilation approaches in general represent a significant improvement on traditional principle component regression (PCR) approaches (Bhend et al., 2012) that are still considered industry standard (PAGES, 2013). One fundamental problem with PCR reconstructions applied over large spatial domains is that they require temporal stability in teleconnection relationships; this does not usually occur in the climate system (Gallant et al., 2013). The MDA approach used to develop PaleoR accommodates non-stationarity by using only the climatic signal at each proxy's location to select analogues from the LME ensemble. MDA accommodates both continuous and non-continuous proxy records and per-

CPD
11, 4159–4204, 2015

mits the simultaneous evaluation of proxies representing different climatic variables and with different seasonal bias: this has been previously a major problem in climate reconstructions (Bradley et al., 2003). As the dynamical relationships between modelled variables are preserved, any modelled variables can potentially be reconstructed. Hence, approaches like PaleoR now provide the best methods to resolve climate variability outside the instrumental era.

4.2 Limitations

The accuracy and quality of all proxy-based research, regardless of methodological considerations, is limited by the quantity, quality and spatial distribution of the proxy data network. Two primary ambiguities relating to the existing proxy dataset are dating uncertainty and non-climatic noise in the proxy signal. In order to address dating uncertainty the reconstructions are produced at a variable resolution that is within estimated dating confidence for the included proxy data. To address signal to noise uncertainty the signals from each proxy are individually evaluated for each time period and only proxies displaying an unambiguous climatic signal are included – as defined by a normalised anomaly of $\pm 0.5\sigma$. There are also many regions of the globe with insufficient proxy data coverage, particularly the Arctic, west Asia, central Africa and central North America – these correspond to the regions of lowest skill in $\text{PaleoR}^{\text{pseudoproxy}}$ evaluation (Fig. 3). Many available proxy records are not yet included in PaleoR and expanding the dataset is an ongoing project.

Another limitation to PaleoR is the current lack of direct tropical SST proxies constraining the assimilation, especially prior to $\sim$ 1550 AD (Fig. 1b). Where there are no actual SST proxies, tropical SST are mostly constrained by proxies sensitive to atmospheric teleconnections (e.g. Fowler et al., 2012). Although the MDA approach makes no prior assumptions about the nature of teleconnection relationships, they need to have been active during the time periods of interest in order for remote proxies to represent tropical SSTa variability. Other uncertainties include potential deficiencies in the

CPD
11, 4159–4204, 2015

model dataset and potential biases in the analogue selection, the next section discusses some potential strategies to address these issues in future versions.

4.3 Planned improvements

PaleoR is our first attempt at producing global paleoclimate reanalysis and is expected to improve significantly with future refinements. In addition to the obvious areas for improvement such as increasing the spatial density of proxy data and experimenting with different model simulations, we have identified several key areas where improvements are planned.

There is significant scope to improve the calibration of proxy and model data. At present proxy records are compared to a single primary modelled climatic variable, either SST, SLP, air temperature or precipitation, this is typically determined by the original published interpretations. However, LME simulates a range of variables that might, in some cases, be more appropriate: such as atmospheric sea salt transport for ice core interpretation; humidity, precipitation-evaporation balance, or streamflow for hydroclimate proxies; and ocean salinity for coral proxies. Some climatic proxies are also sensitive to multiple variables, such as tree-ring growth that is sensitive to both precipitation and temperature (e.g. Fritts, 1976; Villalba, 1990); in these cases simultaneous multivariate calibrations might more appropriate. The emerging technology of proxy system modelling could potentially account for non-climatic influences on proxy signals and might also allow the direct calibration of trace chemical or isotope signals in proxies with equivalent modelled variables (Evans et al., 2013; see Hughes and Ammann, 2009).

Potential biases in the analogue selection have not been directly addressed in this study. Goosse et al. (2006) suggested that a weighting could be applied to each proxy record so that reconstructions favoured proxy records in which higher confidence was placed. The spatial distribution of proxy data is also important; reconstructions could be developed via an iterative or hierarchal approach, whereby regional reconstructions are first produced, then combined into a hemisphere reconstruction. An alternative option

CPD
11, 4159–4204, 2015

could be to apply weights to each proxy depending on its proximity to other records, thereby accounting for differing proxy densities in different regions.

Our focus in this work has been ensuring that PaleoR is consistent with available proxy data (as demonstrated in Fig. 2) and testing the methodology using pseudoproxy experiments (Fig. 3). Verification of PaleoR against the observational record is challenging due to the short overlap period and reduced degrees of freedom associated with a decadally averaged dataset. For example, data-scarcity in the Southern Hemisphere high latitudes mean comparisons with observations are only really valid post ~ 1950 AD. We have recently developed an experimental version of PaleoR at annual resolution over the 1700 to 2000 AD period allowing a more meaningful comparison with the observational record. Initial evaluation is encouraging and we hope to make this dataset available soon. The MDA approach can also accommodate a range of low-resolution proxy data, opening the prospect of exploring periods further in the past, such as the Last Glacial Maximum and Last Inter-Glacial.

5 Conclusions

This article describes the methodology and evaluation of our first attempt at developing a globally relevant paleoclimate reanalysis of the past 1200 years. Our overriding ambition is to make optimum use of both proxy and model data while presenting paleoclimate information in an accessible format suitable for a wide range of research applications. PaleoR is developed using an established "off-line" multivariate data assimilation approach to constrain the LME simulation with a globally distributed proxy dataset. Assimilation of proxy and model data using MDA produces a reanalysis that is highly correlated to almost all included proxy records. PaleoR should therefore provide a reasonable representation of the "real-world" evolution of the climate system – within the limitations of the proxy archive and the model simulation.

Our data assimilation approach offers numerous advantages over conventional PCR based approaches to paleoclimatology. MDA accommodates a wide range of proxy

CPD
11, 4159–4204, 2015

data representing multiple climatic variables, seasonal sensitivities and temporal resolutions, thus optimising the use of available proxy records. MDA is largely unaffected by non-stationarity in covariance relationships. Full spatial fields are reconstructed for multiple variables while preserving dynamical inter–variable relationships. "Off-line" proxy-data assimilation is computationally efficient, easily adaptable to existing climate datasets and easily incorporates new proxy data, thus providing a platform for experimentation, and rapid evaluation of new proxy data and model simulations.

Paleoclimate reanalyses will undoubtedly play a pivotal role in the future of paleoclimatology. PaleoR research and development is an ongoing project, as such we have identified opportunities for potential enhancements in future versions. MDA is just one of many possible approaches to proxy data assimilation and the development of paleoclimate reanalyses. In coming years we will no doubt see the emergence of alternative and possibly more skilful approaches. However, paleoclimate reanalyses will never be as accurate as reanalyses constrained by sufficient meteorological observations – this is simply a reality of dealing with low-resolution high-uncertainty data. Nevertheless, PaleoR has already provided valuable insights into climate system evolution during the past millennium (Goodwin et al., 2013, 2014). The ability to resolve full spatial fields across multiple dynamically consistent variables means PaleoR is a powerful resource for investigating long-term climate variability and the drivers of large-scale climate regime shifts. PaleoR spatial fields for 800 to 2000 AD, as described in this article, can be viewed online at http://climatefutures.mq.edu.au/research/themes/marine/paleor/.

Acknowledgements. This research was part funded by a Macquarie University External Collaborative Grant with the New South Wales Office for Environment and Heritage, and the New South Wales Environmental Trust. S. A. Browning received a postgraduate Macquarie University Research Scholarship (MQRES). The paper draws on a significant proxy climate database, the authors thank all of the researchers and organisations that have retrieved paleoclimate proxy data and had the foresight to make it publicly available.

CPD
11, 4159–4204, 2015

References

Abram, N. J., Mulvaney, R., Wolff, E. W., Triest, J., Kipfstuhl, S., Trusel, L. D., Vimeux, F., Fleet, L., and Arrowsmith, C.: Acceleration of snow melt in an Antarctic Peninsula ice core during the twentieth century, Nat. Geosci., 6, 404–411, doi:10.1038/ngeo1787, 2013.

Abram, N. J., Mulvaney, R., Vimeux, F., Phipps, S. J., Turner, J., and England, M. H.: Evolution of the southern annular mode during the past millennium, Nature Climate Change, 4, 564–569, doi:10.1038/nclimate2235, 2014.

Ammann, C. M. and Wahl, E. R.: The importance of the geophysical context in statistical evaluations of climate reconstruction procedures, Climatic Change, 85, 71–88, doi:10.1007/s10584-007-9276-x, 2007.

Anchukaitis, K. J., D'Arrigo, R. D., Andreu-Hayles, L., Frank, D., Verstege, A., Curtis, A., Buckley, B. M., Jacoby, G. C., and Cook, E. R.: Tree-ring-reconstructed summer temperatures from Northwestern North America during the last nine centuries, J. Climate, 26, 3001–3012, doi:10.1175/JCLI-D-11-00139.1, 2013.

Asami, R., Yamada, T., and Iryu, Y.: Interannual and decadal variability of the western Pacific sea surface condition for the years 1787–2000: Reconstruction based on stable isotope record from a Guam coral, J. Geophys. Res., 110, C05018, doi:10.1029/2004JC002555, 2005.

Ashok, K., Weng, H., and Yamagata, T.: El Nino Modoki and its possible teleconnection, J. Geophys. Res., 112, C11007, doi:10.1029/2006jc003798, 2007.

Bale, R. J., Robertson, I., Salzer, M. W., Loader, N. J., Leavitt, S. W., Gagen, M., Harlan, T. P., and Mccarroll, D.: An annually resolved bristlecone pine carbon isotope chronology for the last millennium, Quaternary Res., 76, 22–29, 2011.

Banta, J. R., McConnell, J. R., Frey, M. M., Bales, R. C., and Taylor, K.: Spatial and temporal variability in snow accumulation at the West Antarctic ice sheet divide over recent centuries, J. Geophys. Res., 113, D23102, doi:10.1029/2008JD010235, 2008.

Barr, C., Tibby, J., Gell, P., Tyler, J., Zawadzki, A., and Jacobsen, G. E.: Climate variability in south-eastern Australia over the last 1500 years inferred from the high-resolution diatom records of two crater lakes, Quaternary Sci. Rev., 95, 115–131, doi:10.1016/j.quascirev.2014.05.001, 2014.

CPD
11, 4159–4204, 2015

Bengtsson, L., Hodges, K. I., Roeckner, E., and Brokopf, R.: On the natural variability of the pre-industrial European climate, Clim. Dynam., 27, 743–760, doi:10.1007/s00382-006-0168-y, 2006.
Bertler, N., Mayewski, P. A., and Carter, L.: Cold conditions in Antarctica during the Little Ice Age – implications for abrupt climate change mechanisms, Earth Planet. Sc. Lett., 308, 41–51, doi:10.1016/j.epsl.2011.05.021, 2011.
Bhend, J., Franke, J., Folini, D., Wild, M., and Brönnimann, S.: An ensemble-based approach to climate reconstructions, Clim. Past, 8, 963–976, doi:10.5194/cp-8-963-2012, 2012.
Bjerknes, J.: A possible response of the atmospheric Hadley circulation to equatorial anomalies of ocean temperature, Tellus A, 18, 820–829, doi:10.3402/tellusa.v18i4.9712, 1966.
Bjerknes, J.: Atmospheric teleconnections from the Equatorial Pacific, Mon. Weather Rev., 97, 163–172, doi:10.1175/1520-0493(1969)097<0163:ATFTEP>2.3.CO;2, 1969.
Black, D. E., Abahazi, M. A., Thunell, R. C., Kaplan, A., Tappa, E. J., and Peterson, L. C.: An 8-century tropical Atlantic SST record from the Cariaco Basin: baseline variability, twentieth-century warming, and Atlantic hurricane frequency, Paleoceanography, 22, PA4204, doi:10.1029/2007PA001427, 2007.
Boiseau, M., Juillet-Leclerc, A., Yiou, P., Salvat, B., Isdale, P., and Guillaume, M.: Atmospheric and oceanic evidences of El Niño–Southern Oscillation events in the south central Pacific Ocean from coral stable isotopic records over the last 137 years, Paleoceanography, 13, 671–685, doi:10.1029/98PA02502, 1998.
Bradley, R. S., Hughes, M. K., and Diaz, H. F.: Climate in Medieval Time, Science, 302, 404–405, doi:10.1126/science.1090372, 2003.
Briffa, K. R., Melvin, T. M., Osborn, T. J., Hantemirov, R. M., Kirdyanov, A. V., Mazepa, V. S., Shiyatov, S. G., and Esper, J.: Reassessing the evidence for tree-growth and inferred temperature change during the common era in Yamalia, northwest Siberia, Quaternary Sci. Rev., 72, 83–107, doi:10.1016/j.quascirev.2013.04.008, 2013.
Browning, S.: The drivers of multidecadal climate variability in the extratropics over the late holocene, PhD thesis, Macquarie University, Sydney, Australia, 2014.
Burns, S. J., Fleitmann, D., Mudelsee, M., Neff, U., Matter, A., and Mangini, A.: A 780 year annually resolved record of Indian Ocean monsoon precipitation from a speleothem from south Oman, J. Geophys. Res-Atmos, 107, D204434, doi:10.1029/2001JD001281, 2002.

CPD
11, 4159–4204, 2015

Büntgen, U., Trouet, V., Frank, D., Leuschner, H. H., Friedrichs, D., Luterbacher, J., and Esper, J.: Tree-ring indicators of German summer drought over the last millennium, Quaternary Sci. Rev., 29, 1005–1016, 2010.

Büntgen, U., Kyncl, T., Ginzler, C., Jacks, D. S., Esper, J., Tegel, W., Heussner, K.-U., and Kyncl, J.: Filling the Eastern European gap in millennium-long temperature reconstructions, P. Natl. A. Sci. USA, 110, 1773–1778, doi:10.1073/pnas.1211485110, 2013.

Casty, C., Wanner, H., Luterbacher, J., Esper, J., and Böhm, R.: Temperature and precipitation variability in the European Alps since 1500, Int. J. Climatol., 25, 1855–1880, doi:10.1002/joc.1216, 2005.

Chen, F. and Yuan, Y.: May–June maximum temperature reconstruction from mean earlywood density in North Central China and its linkages to the summer monsoon activities, PLOS ONE, 9, e107501, doi:10.1371/journal.pone.0107501, 2014.

Christie, D. A., Boninsegna, J. A., Cleaveland, M. K., Lara, A., Le Quesne, C., Morales, M. S., Mudelsee, M., Stahle, D. W., and Villalba, R.: Aridity changes in the Temperate-Mediterranean transition of the Andes since ad 1346 reconstructed from tree-rings, Clim. Dynam., 36, 1505–1521, doi:10.1007/s00382-009-0723-4, 2009.

Clapperton, C. M.: Quaternary glaciations in the Southern Ocean and Antarctic peninsula area, Quaternary Sci. Rev., 9, 229–252, doi:10.1016/0277-379190020-B, 1990.

Cleaveland, M. K., Votteler, T. H., Stahle, D. K., Casteel, R. C., and Banner, J. L.: Extended chronology of drought in South Central, Southeastern and West Texas, Texas Water Journal, 2, 54–96, 2011.

Cobb, K. M., Charles, C. D., Cheng, H., and Edwards, R. L.: El Nino/Southern Oscillation and tropical Pacific climate during the last millennium, Nature, 424, 271–276, doi:10.1038/nature01779, 2003.

Cohen, T. J., Nanson, G. C., Jansen, J. D., Jones, B. G., Jacobs, Z., Treble, P., Price, D. M., May, J. H., Smith, A. M., and Ayliffe, L. K.: Continental aridification and the vanishing of Australia's megalakes, Geology, 39, 167–170, doi:10.1130/G31518.1, 2011.

Cohen, T. J., Nanson, G. C., Jansen, J. D., Gliganic, L. A., May, J. H., Larsen, J. R., Goodwin, I. D., Browning, S., and Price, D. M.: A pluvial episode identified in arid Australia during the Medieval climatic anomaly, Quaternary Sci. Rev., 56, 167–171, doi:10.1016/j.quascirev.2012.09.021, 2012.

Cole, J.: Tropical Pacific forcing of decadal SST variability in the Western Indian Ocean over the past two centuries, Science, 287, 617–619, doi:10.1126/science.287.5453.617, 2000.

CPD
11, 4159–4204, 2015

Compo, G. P., Whitaker, J. S., Sardeshmukh, P. D., Matsui, N., Allan, R. J., Yin, X., Gleason, B. E., Vose, R. S., Rutledge, G., and Bessemoulin, P.: The twentieth century reanalysis project, Q. J. Roy. Meteor. Soc., 137, 1–28, doi:10.1002/qj.776, 2011.

Conroy, J. L., Overpeck, J. T., Cole, J. E., Shanahan, T. M., and Steinitz-Kannan, M.: Holocene changes in eastern tropical Pacific climate inferred from a Galápagos lake sediment record, Quaternary Sci. Rev., 27, 1166–1180, doi:10.1016/j.quascirev.2008.02.015, 2008.

Cook, E. R., Meko, D. M., Stahle, D. W., and Cleaveland, M. K.: Drought reconstructions for the continental United States, J. Climate, 12, 1145–1162, doi:10.1175/1520-0442(1999)012<1145:DRFTCU>2.0.CO;2, 1999.

Cook, E. R., Palmer, J. G., and D'Arrigo, R. D.: Evidence for a "Medieval Warm Period" in a 1,100 year tree-ring reconstruction of past austral summer temperatures in New Zealand, Geophys. Res. Lett., 29, 1667, doi:10.1029/2001gl014580, 2002.

Cook, E. R., Krusic, P. J., and Jones, P. D.: Dendroclimatic signals in long tree-ring chronologies from the Himalayas of Nepal, Int. J. Climatol., 23, 707–732, doi:10.1002/joc.911, 2003.

Cook, E. R., Woodhouse, C. A., Eakin, C. M., Meko, D. M., and Stahle, D. W.: Long-term aridity changes in the western United States, Science, 306, 1015–1018, doi:10.1126/science.1102586, 2004.

Cook, E. R., Buckley, B. M., Palmer, J. G., and Boswijk, G.: Millennia-long tree-ring records from Tasmania and New Zealand: a basis for modelling climate variability and forcing, past, present and future, J. Quaternary Sci., 21, 689–699, doi:10.1002/jqs.1071, 2006.

Cronin, T. M., Dwyer, G. S., Kamiya, T., Schwede, S., and Willard, D. A.: Medieval warm period, little ice age and 20th century temperature variability from Chesapeake Bay, Global Planet. Change, 36, 17–29, 2003.

Cullen, L. E. and Grierson, P. F.: Multi-decadal scale variability in autumn-winter rainfall in south-western Australia since 1655 AD as reconstructed from tree rings of *Callitris columellaris*, Clim. Dynam., 33, 433–444, doi:10.1007/s00382-008-0457-8, 2008.

Cunningham, S. A., Roberts, C. D., Frajka-Williams, E., Johns, W. E., Hobbs, W., Palmer, M. D., Rayner, D., Smeed, D. A., and McCarthy, G.: Atlantic meridional overturning circulation slowdown cooled the subtropical ocean, Geophys. Res. Lett., 40, 6202–6207, doi:10.1002/2013GL058464, 2013.

D'Arrigo, R., Cook, E., Palmer, J., Krusic, P., Buckley, B., and Villalba, R.: Tree-ring records from New Zealand: long-term context for recent warming trend, Clim. Dynam., 14, 191–199, doi:10.1007/s003820050217, 1998.

CPD
11, 4159–4204, 2015

D'Arrigo, R., Villalba, R., Buckley, B., Salinger, J., Palmer, J., and Allen, K.: Trans-Tasman Sea climate variability since ad 1740 inferred from middle to high latitude tree-ring data – springer, Clim. Dynam., 16, 603–610, doi:10.1007/s003820000070, 2000.

Damassa, T. D., Cole, J. E., Barnett, H. R., Ault, T. R., and McClanahan, T. R.: Enhanced multidecadal climate variability in the seventeenth century from coral isotope records in the western Indian Ocean, Paleoceanography, 21, PA2016, doi:10.1029/2005PA001217, 2006.

Davi, N., D'Arrigo, R., Jacoby, G., Buckley, B., and Kobayashi, O.: Warm-season annual to decadal temperature variability for Hokkaido, Japan, inferred from maximum latewood density and ring width data, Climatic Change, 52, 201–217, doi:10.1023/A:1013085624162, 2002.

Davi, N. K., Jacoby, G. C., Curtis, A. E., and Baatarbileg, N.: Extension of drought records for Central Asia using tree rings: West-Central Mongolia, J. Climate, 19, 288–299, doi:10.1175/JCLI3621.1, 2006.

Davi, N. K., Pederson, N., Leland, C., Nachin, B., Suran, B., and Jacoby, G. C.: Is eastern Mongolia drying? A long-term perspective of a multidecadal trend, Water Resour. Res., 49, 151–158, 2013.

Dee, D. P., Uppala, S. M., Simmons, A. J., Berrisford, P., Poli, P., Kobayashi, S., Andrae, U., Balmaseda, M. A., Balsamo, G., Bauer, P., Bechtold, P., Beljaars, A. C. M., van de Berg, L., Bidlot, J., Bormann, N., Delsol, C., Dragani, R., Fuentes, M., Geer, A. J., Haimberger, L., Healy, S. B., Hersbach, H., Hólm, E. V., Isaksen, L., Kållberg, P., Köhler, M., Matricardi, M., McNally, A. P., Monge-Sanz, B. M., Morcrette, J. J., Park, B. K., Peubey, C., de Rosnay, P., Tavolato, C., Thépaut, J. N., and Vitart, F.: The ERA-interim reanalysis: configuration and performance of the data assimilation system, Q. J. Roy. Meteor. Soc., 137, 553–597, doi:10.1002/qj.828, 2011.

DeLong, K. L., Flannery, J. A., Poore, R. Z., Quinn, T. M., Maupin, C. R., Lin, K., and Shen, C.-C.: A reconstruction of sea surface temperature variability in the southeastern Gulf of Mexico from 1734 to 2008 C. E. using cross-dated Sr/Ca records from the coral *Siderastrea siderea*, Paleoceanography, 29, 403–422, doi:10.1002/2013PA002524, 2014.

DeLong, K. L., Quinn, T. M., Taylor, F. W., Lin, K., and Shen, C.-C.: Sea surface temperature variability in the southwest tropical Pacific since AD 1649, Nature Climate Change, 2, 799–804, doi:10.1038/nclimate1583, 2012.

CPD
11, 4159–4204, 2015

Eichler, A., Olivier, S., Henderson, K., Laube, A., Beer, J., Papina, T., Gäggeler, H. W., and Schwikowski, M.: Temperature response in the Altai region lags solar forcing, Geophys. Res. Lett., 36, L01808, doi:10.1029/2008GL035930, 2009.

Elbert, J., Grosjean, M., von Gunten, L., Urrutia, R., Fischer, D., Wartenburger, R., Ariztegui, D., Fujak, M., and Hamann, Y.: Quantitative high-resolution winter (JJA) precipitation reconstruction from varved sediments of Lago Plomo 47 S, Patagonian Andes, AD 1530–2002, Holocene, 22, 465–474, doi:10.1177/0959683611425547, 2012.

Emile-Geay, J. and Eshleman, J. A.: Toward a semantic web of paleoclimatology, Geochem. Geophy. Geosy., 14, 457–469, doi:10.1002/ggge.20067, 2013.

Emile-Geay, J., Cobb, K. M., Mann, M. E., and Wittenberg, A. T.: Estimating central equatorial Pacific SST variability over the past millennium, Part I: methodology and validation, J. Climate, 26, 2302–2328, doi:10.1175/JCLI-D-11-00510.1, 2013a.

Emile-Geay, J., Cobb, K. M., Mann, M. E., and Wittenberg, A. T.: Estimating Central Equatorial Pacific SST variability over the Past Millennium, Part II: Reconstructions and implications, J. Climate, 26, 2329–2352, doi:10.1175/JCLI-D-11-00511.1, 2013b.

Esper, J., Dunthorn, E., Krusic, P. J., Timonen, M., and Büntgen, U.: Northern European summer temperature variations over the Common Era from integrated tree-ring density records, J. Quaternary Sci., 29, 487–494, doi:10.1002/jqs.2726, 2014.

Esper, J., Frank, D., Büntgen, U., Verstege, A., Luterbacher, J., and Xoplaki, E.: Long-term drought severity variations in Morocco, Geophys. Res. Lett., 34, L17702, doi:10.1029/2007GL030844, 2007.

Evans, M. N., Tolwinski-Ward, S. E., Thompson, D. M., and Anchukaitis, K. J.: Applications of proxy system modeling in high resolution paleoclimatology, Quaternary Sci. Rev., 76, 16–28, doi:10.1016/j.quascirev.2013.05.024, 2013.

Fisher, D. A., Koerner, R. M., and Reeh, N.: Holocene climatic records from Agassiz Ice Cap, Ellesmere Island, NWT, Canada, Holocene, 5, 19–24, doi:10.1177/095968369500500103, 1995.

Fogt, R. L. and Bromwich, D. H.: Decadal variability of the ENSO teleconnection to the high-latitude South Pacific governed by coupling with the southern annular mode, J. Climate, 19, 979–997, doi:10.1175/JCLI3671.1, 2006.

Fowler, A., Boswijk, G., Gergis, J., and Lorrey, A.: ENSO history recorded in Agathis australis (kauri) tree rings, Part A: kauri's potential as an ENSO proxy, Int. J. Climatol., 28, 1–20, doi:10.1002/joc.1525, 2008.

CPD
11, 4159–4204, 2015

Fowler, A. M., Boswijk, G., Lorrey, A. M., Pirie, M., McCloskey, S. P. J., Palmer, J. G., and Wunder, J.: Multi-centennial tree-ring record of ENSO-related activity in New Zealand, Nature Climate Change, 2, 172–176, doi:10.1038/nclimate1374, 2012.

Franke, J., González-Rouco, J. F., Frank, D., and Graham, N. E.: 200 years of European temperature variability: insights from and tests of the proxy surrogate reconstruction analog method, Clim. Dynam., 37, 133–150, doi:10.1007/s00382-010-0802-6, 2010.

Fritts, H. C.: Tree Rings and Climate, Academic press, London, 1976.

Gallant, A. J. E., Phipps, S. J., Karoly, D. J., Mullan, A. B., and Lorrey, A. M.: Nonstationary Australasian teleconnections and implications for Paleoclimate reconstructions, J. Climate, 26, 8827–8849, doi:10.1175/JCLI-D-12-00338.1, 2013.

Garcin, Y., Vincens, A., Williamson, D., Buchet, G., and Guiot, J.: Abrupt resumption of the African monsoon at the younger dryas – Holocene climatic transition, Quaternary Sci. Rev., 26, 690–704, doi:10.1016/j.quascirev.2006.10.014, 2007.

Gennaretti, F., Arseneault, D., Nicault, A., Perreault, L., and Bégin, Y.: Volcano-induced regime shifts in millennial tree-ring chronologies from northeastern North America, P. Natl. A. Sci. USA, 111, 10077–10082, doi:10.1073/pnas.1324220111, 2014.

Goodkin, N. F., Hughen, K. A., Curry, W. B., Doney, S. C., and Ostermann, D. R.: Sea surface temperature and salinity variability at Bermuda during the end of the Little Ice Age, Paleoceanography, 23, PA3203, doi:10.1029/2007PA001532, 2008.

Goodwin, I., Browning, S., Lorrey, A., Mayewski, P., Phipps, S., Bertler, N. N., Edwards, R., Cohen, T., van Ommen, T., Curran, M., Barr, C., and Stager, J. C.: A reconstruction of extra-tropical Indo-Pacific sea-level pressure patterns during the Medieval climate anomaly, Clim. Dynam., 43, 1197–1219, doi:10.1007/s00382-013-1899-1, 2013.

Goodwin, I. D. and Harvey, N.: Subtropical sea-level history from coral microatolls in the Southern Cook Islands, since 300 AD, Mar. Geol., 253, 14–25, doi:10.1016/j.margeo.2008.04.012, 2008.

Goodwin, I. D., Van Ommen, T. D., Curran, M., and Mayewski, P. A.: Mid latitude winter climate variability in the South Indian and southwest Pacific regions since 1300 AD, Clim. Dynam., 22, 783–794, doi:10.1007/s00382-004-0403-3, 2004.

Goodwin, I. D., Stables, M. A., and Olley, J. M.: Wave climate, sand budget and shoreline alignment evolution of the Iluka–Woody Bay sand barrier, northern New South Wales, Australia, since 3000 yr BP, Mar. Geol., 226, 127–144, doi:10.1016/j.margeo.2005.09.013, 2006.

CPD
11, 4159–4204, 2015

Goodwin, I. D., Browning, S. A., and Anderson, A. J.: Climate windows for Polynesian voyaging to New Zealand and Easter Island, P. Natl. A. Sci. USA, 111, 14716–14721, doi:10.1073/pnas.1408918111, 2014.
Goosse, H., Renssen, H., Timmermann, A., Bradley, R. S., and Mann, M. E.: Using paleoclimate proxy-data to select optimal realisations in an ensemble of simulations of the climate of the past millennium, Clim. Dynam., 27, 165–184, doi:10.1007/s00382-006-0128-6, 2006.
Goosse, H., Crespin, E., de Montety, A., Mann, M. E., Renssen, H., and Timmermann, A.: Reconstructing surface temperature changes over the past 600 years using climate model simulations with data assimilation, J. Geophys. Res., 115, D09108, doi:10.1029/2009JD012737, 2010.
Graf, H.-F., and Zanchettin, D.: Central Pacific El Niño, the "subtropical bridge," and Eurasian climate, J. Geophys. Res-Atmos, 117, D01102, doi:10.1029/2011JD016493, 2012.
Graham, N. E., Hughes, M. K., Ammann, C. M., Cobb, K. M., Hoerling, M. P., Kennett, D. J., Kennett, J. P., Rein, B., Stott, L., Wigand, P. E., and Xu, T.: Tropical Pacific – mid-latitude teleconnections in medieval times, Climatic Change, 83, 241–285, doi:10.1007/s10584-007-9239-2, 2007.
Griffiths, M. L., Gagan, M. K., Zhao, J. X., Ayliffe, L. K., Hantoro, W. S., Frisia, S., Feng, Y. X., Cartwright, I., Pierre, E. S., Fischer, M. J., and Suwargadi, B. W.: Increasing Australian–Indonesian monsoon rainfall linked to early Holocene sea-level rise, Nat. Geosci., 2, 636–639, doi:10.1038/ngeo605, 2009.
Griggs, C., DeGaetano, A., Kuniholm, P., and Newton, M.: A regional high-frequency reconstruction of May–June precipitation in the north Aegean from oak tree rings, A. D. 1089–1989, Int. J. Climatol., 27, 1075–1089, doi:10.1002/joc.1459, 2007.
Gunnarson, B. E., Linderholm, H. W., and Moberg, A.: Improving a tree-ring reconstruction from west-central Scandinavia: 900 years of warm-season temperatures, Clim. Dynam., 36, 97–108, doi:10.1007/s00382-010-0783-5, 2010.
Hakim, G. J., Annan, J. D., Brönnimann, S., Crucifix, M., Edwards, T., Goosse, H., Paul, A., van der Schrier, G., and Widmann, M.: Overview of data assimilation methods, PAGES News, 21, 72–73, 2013.
Helama, S., Vartiainen, M., Holopainen, J., Mäkelä, H. M., Kolström, T., and Meriläinen, J.: A palaeotemperature record for the Finnish Lakeland based on microdensitometric variations in tree rings, Geochron., 41, 265–277, doi:10.2478/s13386-013-0163-0, 2014.

CPD
11, 4159–4204, 2015

Hendy, E. J., Gagan, M. K., Alibert, C. A., McCulloch, M. T., Lough, J. M., and Isdale, P. J.: Abrupt decrease in tropical Pacific sea surface salinity at end of Little Ice Age, Science, 295, 1511–1514, doi:10.1126/science.1067693, 2002.

Hendy, E. J., Gagan, M. K., and Lough, J. M.: Chronological control of coral records using luminescent lines and evidence for non-stationary ENSO teleconnections in northeast Australia, Holocene, 13, 187–199, doi:10.1191/0959683603hl606rp, 2003.

Ho, M., Kiem, A. S., and Verdon-Kidd, D. C.: The southern annular mode: a comparison of indices, Hydrol. Earth Syst. Sc., 8, 7461–7498, doi:10.5194/hessd-8-7461-2011, 2011.

Holmgren, K., Karlen, W., Svanered, O., Lauritzen, S. E., Lee Thorp, J. A., Partridge, T. C., Piketh, S., and Tyson, P. D.: A 3000 year high-resolution stalagmite-based record of palaeoclimate for northeastern South Africa, Holocene, 9, 295–309, doi:10.1191/095968399672625464, 1999.

Hughes, M. K. and Ammann, C. M.: The future of the past – an earth system framework for high resolution paleoclimatology: editorial essay, Climatic Change, 94, 247–259, doi:10.1007/s10584-009-9588-0, 2009.

Hurrell, J. W.: Decadal trends in the North Atlantic oscillation: regional temperatures and precipitation, Science, 269, 676–679, doi:10.1126/science.269.5224.676, 1995.

Hurrell, J. W. and Deser, C.: North Atlantic climate variability: the role of the North Atlantic Oscillation, J. Marine Syst., 78, 28–41, doi:10.1016/j.jmarsys.2008.11.026, 2009.

Johnson, T. C., Barry, S. L., Chan, Y., and Wilkinson, P.: Decadal record of climate variability spanning the past 700 yr in the Southern Tropics of East Africa, Geology, 29, 83, doi:10.1130/0091-7613(2001)029<0083:DROCVS>2.0.CO;2, 2001.

Jones, P. D., Briffa, K. R., Osborn, T. J., Lough, J. M., Van Ommen, T. D., Vinther, B. M., Luterbacher, J., Wahl, E. R., Zwiers, F. W., Mann, M. E., Ammann, C. M., Buckley, B. M., Cobb, K. M., Esper, J., Graham, N., Küttel, M., Mosley-Thompson, E., Overpeck, J. T., Tudhope, A. W., Villalba, R., Wanner, H., and Xoplaki, E.: High-resolution palaeoclimatology of the last millennium: a review of current status and future prospects, Holocene, 19, 3–49, doi:10.1177/0959683608098952, 2009.

Kalnay, E., Kanamitsu, M., Kistler, R., Collins, W., Deaven, D., Gandin, L., Iredell, M., Saha, S., White, G., Woollen, J., Zhu, Y., Leetmaa, A., Reynolds, R., Chelliah, M., Ebisuzaki, W., Higgins, W., Janowiak, J., MO, K. C., Ropelewski, C., Wang, J., Jenne, R., and Joseph, D.: The NCEP/NCAR 40 year reanalysis project, B. Am. Meteorol. Soc., 77, 437–471, doi:10.1175/1520-0477(1996)077<0437:TNYRP>2.0.CO;2, 1996.

CPD
11, 4159–4204, 2015

Kilbourne, K. H., Quinn, T. M., Webb, R., Guilderson, T., Nyberg, J., and Winter, A.: Paleoclimate proxy perspective on Caribbean climate since the year 1751: Evidence of cooler temperatures and multidecadal variability, Paleoceanography, 23, PA3220, doi:10.1029/2008PA001598, 2008.

Kobashi, T., Kawamura, K., Severinghaus, J. P., Barnola, J.-M., Nakaegawa, T., Vinther, B. M., Johnsen, S. J., and Box, J. E.: High variability of greenland surface temperature over the past 4000 years estimated from trapped air in an ice core, Geophys. Res. Lett., 38, L21501, doi:10.1029/2011GL049444, 2011.

Kreutz, K. J., Mayewski, P. A., Pittalwala, I. I., Meeker, L. D., Twickler, M. S., and Whitlow, S. I.: Sea level pressure variability in the Amundsen Sea region inferred from a West Antarctic glaciochemical record, J. Geophys. Res., 105, 4047–4059, doi:10.1029/1999JD901069, 2000.

Kuhnert, H., Patzold, J., Hatcher, B., Wyrwoll, K., Eisenhauer, A., Collins, L. B., Zhu, Z. R., and Wefer, G.: A 200 year coral stable oxygen isotope record from a high-latitude reef off Western Australia, Coral Reefs, 18, 1–12, doi:10.1007/s003380050147, 1999.

Lau, N.-C.: Interactions between global SST anomalies and the midlatitude atmospheric circulation, B. Am. Meteorol. Soc., 78, 21–33, doi:10.1175/1520-0477(1997)078<0021:IBGSAA>2.0.CO;2, 1997.

Le Quesne, C., Stahle, D. W., Cleaveland, M. K., Therrell, M. D., and Aravena, J. C.: Ancient austrocedrustree-ring chronologies used to reconstruct Central Chile precipitation variability from a.d. 1200 to 2000, J. Climate, 19, 5731–5744, doi:10.1175/JCLI3935.1, 2006.

Li, B. and Smerdon, J. E.: Defining spatial comparison metrics for evaluation of paleoclimatic field reconstructions of the Common Era, Environmetrics, 23, 394–406, doi:10.1002/env.2142, 2012.

Linsley, B. K., Dunbar, R. B., Wellington, G. M., and Mucciarone, D. A.: A coral-based reconstruction of intertropical convergence zone variability over Central America since 1707, J. Geophys. Res., 99, 9977–9977, 1994.

Linsley, B. K., Zhang, P., Kaplan, A., Howe, S. S., and Wellington, G. M.: Interdecadal-decadal climate variability from multicoral oxygen isotope records in the South Pacific convergence zone region since 1650 A.D, Paleoceanography, 23, PA2219, doi:10.1029/2007PA001539, 2008.

CPD
11, 4159–4204, 2015

Lorrey, A., Salinger, J., Palmer, J., and Neil, H.: Speleothem stable isotope records interpreted within a multi-proxy framework and implications for New Zealand palaeoclimate reconstruction, Quatern. Int., 187, 52–75, doi:10.1016/j.quaint.2007.09.039, 2008.

Lough, J. M.: Great Barrier Reef coral luminescence reveals rainfall variability over northeastern Australia since the 17th century, Paleoceanography, 26, PA2201, doi:10.1029/2010PA002050, 2011.

Luckman, B. H. and Wilson, R. J. S.: Summer temperatures in the Canadian Rockies during the last millennium: a revised record, Clim. Dynam., 24, 131–144, doi:10.1007/s00382-004-0511-0, 2005.

Malevich, S. B., Woodhouse, C. A., and Meko, D. M.: Tree-ring reconstructed hydroclimate of the upper Klamath basin, J. Hydrol., 495, 13–22, doi:10.1016/j.jhydrol.2013.04.048, 2013.

Mann, M., Rutherford, S., Wahl, E., and Ammann, C. M.: Robustness of proxy-based climate field reconstruction methods, J. Geophys. Res., 112, D12109, doi:10.1029/2006jd008272, 2007.

Mann, M. E., Rutherford, S., Wahl, E., and Ammann, C.: Testing the fidelity of methods used in proxy-based reconstructions of past climate, J. Climate, 18, 4097–4107, doi:10.1175/JCLI3564.1, 2005.

Martín-Chivelet, J., Muñoz-García, M. B., Edwards, R. L., Turrero, M. J., and Ortega, A. I.: Land surface temperature changes in Northern Iberia since 4000yr BP, based on $\delta^{13}C$ of speleothems, Global Planet. Change, 77, 1–12, doi:10.1016/j.gloplacha.2011.02.002, 2011.

Maupin, C. R., Partin, J. W., Shen, C.-C., Quinn, T. M., Lin, K., Taylor, F. W., Banner, J. L., Thirumalai, K., and Sinclair, D. J.: Persistent decadal-scale rainfall variability in the tropical South Pacific convergence zone through the past six centuries, Clim. Past, 10, 1319–1332, doi:10.5194/cp-10-1319-2014, 2014.

Maxwell, R. S., Hessl, A. E., Cook, E. R., and Pederson, N.: A multispecies tree ring reconstruction of Potomac River streamflow (950–2001), Water Resour. Res., 47, W05512, doi:10.1029/2010WR010019, 2011.

Maxwell, R. S., Hessl, A. E., Cook, E. R., and Buckley, B. M.: A multicentury reconstruction of may precipitation for the Mid-Atlantic region using juniperus virginiana tree rings, J. Climate, 25, 1045–1056, doi:10.1175/JCLI-D-11-00017.1, 2012.

McGregor, S., Timmermann, A., and Timm, O.: A unified proxy for ENSO and PDO variability since 1650, Clim. Past, 6, 1–17, doi:10.5194/cp-6-1-2010, 2010.

CPD
11, 4159–4204, 2015

Meko, D. M., Woodhouse, C. A., Baisan, C. A., Knight, T., Lukas, J. J., Hughes, M. K., and Salzer, M. W.: Medieval drought in the upper Colorado River Basin, Geophys. Res. Lett., 34, L10705, doi:10.1029/2007GL029988, 2007.

Mo, K. C. and Ghil, M.: Statistics and dynamics of persistent anomalies, J. Atmos. Sci., 44, 877–902, doi:10.1175/1520-0469(1987)044<0877:SADOPA>2.0.CO;2, 1987.

Mo, K. C. and Higgins, R. W.: The Pacific-South American modes and tropical convection during the Southern Hemisphere winter, Mon. Weather Rev., 126, 1581–1596, doi:10.1175/1520-0493(1998)126<1581:TPSAMA>2.0.CO;2, 1998.

Moy, C. M., Dunbar, R. B., Moreno, P. I., Mucciarone, D. M., Guilderson, T. P., and Garreaud, R. D.: Isotopic evidence for hydrologic change related to the westerlies in SW Patagonia, Chile, during the last millennium, Quaternary Sci. Rev., 27, 1335–1349, doi:10.1016/j.quascirev.2008.03.006, 2008.

National Center for Atmospheric Research Staff (Eds.): The Climate Data Guide: Hurrell North Atlantic Oscillation (NAO) Index (PC-based), last modified 07 July 2015, available at: https://climatedataguide.ucar.edu/climate-data/hurrell-north-atlantic-oscillation-nao-index-pc-based (8 July 2015), 2015.

Neukom, R., Luterbacher, J., Villalba, R., Frank, D., Grosjean, M., Esper, J., and Wanner, H.: Multi-centennial summer and winter precipitation variability in southern South America, Geophys. Res. Lett., 37, L14708, doi:10.1029/2010gl043680, 2010a.

Neukom, R., Luterbacher, J., Villalba, R., Küttel, M., Frank, D., Jones, P. D., Grosjean, M., Wanner, H., Aravena, J.-C., and D'Arrigo, R.: Multiproxy summer and winter surface air temperature field reconstructions for southern South America covering the past centuries, Clim. Dynam., 37, 35–51, doi:10.1007/s00382-010-0793-3, 2010b.

Newman, M., Shin, S., and Alexander, M. A.: Natural variation in ENSO flavors, Geophys. Res. Lett., 38, L14705, doi:10.1029/2011GL047658, 2011.

Noon, P. E., Leng, M. J., and Jones, V. J.: Oxygen-isotope (δ18O) evidence of Holocene hydrological changes at Signy Island, maritime Antarctica, Holocene, 13, 251–263, doi:10.1191/0959683603hl611rp, 2003.

Oerter, H., Kipfstuhl, S., and Wilhelms, F.: Stable Isotope Records for the Past 1000 years from Five Ice Cores in Central Dronning Maud Land, IUGG, 2011.

Ortega, P., Lehner, F., Swingedouw, D., Masson-Delmotte, V., Raible, C. C., Casado, M., and Yiou, P.: A model-tested North Atlantic Oscillation reconstruction for the past millennium, Nature, 523, 71–74, doi:10.1038/nature14518, 2015.

CPD
11, 4159–4204, 2015

Otto-Bliesner, B. L., Brady, E. C., Fasullo, J., Jahn, A., Landrum, L., Stevenson, S., Rosenbloom, N., Mai, A., and Strand, G.: Climate Variability and Change since 850 C. E.: An ensemble approach with the community earth system model (CESM), B. Am. Meteorol. Soc., in press, doi:10.1175/BAMS-D-14-00233.1, 2015.

PAGES, 2 K. Consortium: Continental-scale temperature variability during the past two millennia, Nat. Geosci., 6, 339–346, doi:10.1038/ngeo1797, 2013.

Partin, J. W., Quinn, T. M., Shen, C.-C., Emile-Geay, J., Taylor, F. W., Maupin, C. R., Lin, K., Jackson, C. S., Banner, J. L., and Sinclair, D. J.: Multidecadal rainfall variability in South Pacific convergence zone as revealed by stalagmite geochemistry, Geology, 41, 1143–1146, doi:10.1130/G34718.1, 2013.

Pederson, N., Leland, C., Nachin, B., Hessl, A. E., Bell, A. R., Martin-Benito, D., Saladyga, T., Suran, B., Brown, P. M., and Davi, N. K.: Three centuries of shifting hydroclimatic regimes across the Mongolian Breadbasket, Agr. Forest Meteorol., 178–179, 10–20, doi:10.1016/j.agrformet.2012.07.003, 2013.

Proctor, C., Baker, A., and Barnes, W.: A three thousand year record of North Atlantic climate, Clim. Dynam., 19, 449–454, doi:10.1007/s00382-002-0236-x, 2002.

Quinn, T. M., Taylor, F. W., and Crowley, T. J.: A 173 year stable isotope record from a tropical south pacific coral, Quaternary Sci. Rev., 12, 407–418, doi:10.1016/S0277-379180005-8, 1993.

Rhodes, R. H., Bertler, N. A. N., Baker, J. A., Steen-Larsen, H. C., Sneed, S. B., Morgenstern, U., and Johnsen, S. J.: Little Ice Age climate and oceanic conditions of the Ross Sea, Antarctica from a coastal ice core record, Clim. Past, 8, 1223–1238, doi:10.5194/cp-8-1223-2012, 2012.

Saenger, C., Cohen, A. L., Oppo, D. W., Halley, R. B., and Carilli, J. E.: Surface-temperature trends and variability in the low-latitude North Atlantic since 1552, Nat. Geosci., 2, 492–495, doi:10.1038/ngeo552, 2009.

Salzer, M. W. and Kipfmueller, K. F.: Reconstructed temperature and precipitation on a millennial timescale from tree-rings in the Southern Colorado Plateau, USA, Climatic Change, 70, 465–487, doi:10.1007/s10584-005-5922-3, 2005.

Salzer, M. W., Bunn, A. G., Graham, N. E., and Hughes, M. K.: Five millennia of paleotemperature from tree-rings in the Great Basin, USA, Clim. Dynam., 42, 1517–1526, doi:10.1007/s00382-013-1911-9, 2013.

CPD
11, 4159–4204, 2015

Schaefer, J. M., Denton, G. H., Kaplan, M., Putnam, A., Finkel, R. C., Barrell, D. J., Andersen, B. G., Schwartz, R., Mackintosh, A., and Chinn, T.: High-frequency Holocene glacier fluctuations in New Zealand differ from the northern signature, Science, 324, 622–625, doi:10.1126/science.1169312, 2009.

Schenk, F. and Zorita, E.: Reconstruction of high resolution atmospheric fields for Northern Europe using analog-upscaling, Clim. Past, 8, 1681–1703, doi:10.5194/cp-8-1681-2012, 2012.

Smerdon, J. E., Kaplan, A., and Amrhein, D. E.: Reply to "Comments on 'Erroneous Model Field Representations in Multiple Pseudoproxy Studies: Corrections and Implications'*, J. Climate, 26, 3485–3486, doi:10.1175/JCLI-D-12-00165.1, 2013.

Stager, J. C., Mayewski, P. A., White, J., Chase, B. M., Neumann, F. H., Meadows, M. E., King, C. D., and Dixon, D. A.: Precipitation variability in the winter rainfall zone of South Africa during the last 1400 yr linked to the austral westerlies, Clim. Past, 8, 877–887, doi:10.5194/cp-8-877-2012, 2012.

Stahle, D. W., Diaz, J. V., Burnette, D. J., Paredes, J. C., Heim Jr., R. R., Fye, F. K., Acuna Soto, R., Therrell, M. D., Cleaveland, M. K., and Stahle, D. K.: Major Mesoamerican droughts of the past millennium, Geophys. Res. Lett., 38, L05703, doi:10.1029/2010GL046472, 2011.

Steiger, N. J., Hakim, G. J., Steig, E. J., Battisti, D. S., and Roe, G. H.: Assimilation of time-averaged pseudoproxies for climate reconstruction, J. Climate, 27, 426–441, doi:10.1175/JCLI-D-12-00693.1, 2013.

Steinman, B. A., Abbott, M. B., Mann, M. E., Stansell, N. D., and Finney, B. P.: 1500 year quantitative reconstruction of winter precipitation in the Pacific Northwest, P. Natl. A. Sci. USA, 109, 11619–11623, doi:10.1073/pnas.1201083109, 2012.

Sundqvist, H. S., Holmgren, K., Fohlmeister, J., Zhang, Q., Matthews, M. B., Spötl, C., and Kornich, H.: Evidence of a large cooling between 1690 and 1740 AD in southern Africa, Sci. Rep., 3, 1767, doi:10.1038/srep01767, 2013.

Tan, L., Cai, Y., An, Z., Yi, L., Zhang, H., and Qin, S.: Climate patterns in north central China during the last 1800 yr and their possible driving force, Clim. Past, 7, 685–692, doi:10.5194/cp-7-685-2011, 2011.

Tan, M.: Cyclic rapid warming on centennial-scale revealed by a 2650 year stalagmite record of warm season temperature, Geophys. Res. Lett., 30, 1617, doi:10.1029/2003GL017352, 2003.

Therrell, M. D., Stahle, D. W., Ries, L. P., and Shugart, H. H.: Tree-ring reconstructed rainfall variability in Zimbabwe, Clim. Dynam., 26, 677–685, doi:10.1007/s00382-005-0108-2, 2006.

CPD
11, 4159–4204, 2015

Thomas, E. K. and Briner, J. P.: Clim. Past millennium inferred from varved proglacial lake sediments on northeast Baffin Island, Arctic Canada, J. Paleolimnol., 41, 209–224, doi:10.1007/s10933-008-9258-7, 2009.

Thompson, L. G.: Quelccaya ice core database IGBP PAGES/World data center – a for Paleoclimatology data contribution series # 92–008, NOAA/NGDC Paleoclimatology Program, Boulder CO, USA, 1992.

Thompson, L. G., Mosley-Thompson, E., Brecher, H., Davis, M., León, B., Les, D., Lin, P.-N., Mashiotta, T., and Mountain, K.: Abrupt tropical climate change: past and present, P. Natl. A. Sci. USA, 103, 10536–10543, doi:10.1073/pnas.0603900103, 2006.

Trachsel, M., Kamenik, C., Grosjean, M., McCarroll, D., Moberg, A., Brázdil, R., Büntgen, U., Dobrovolný, P., Esper, J., Frank, D. C., Friedrich, M., Glaser, R., Larocque-Tobler, I., Nicolussi, K., and Riemann, D.: Multi-archive summer temperature reconstruction for the European Alps, AD 1053–1996, Quaternary Sci. Rev., 46, 66–79, doi:10.1016/j.quascirev.2012.04.021, 2012.

Trenberth, K., Stepaniak, D., and Smith, L.: Interannual variability of patterns of atmospheric mass distribution, J. Climate, 18, 2812–2825, doi:10.1175/JCLI3333.1, 2005.

Trenberth, K. E.: The definition of El Nino, B. Am. Meteorol. Soc., 78, 2771–2777, doi:10.1175/1520-0477(1997)078<2771:TDOENO>2.0.CO;2, 1997.

Trouet, V., Esper, J., and Frank, D.: Persistent positive North Atlantic oscillation mode dominated the Medieval climate anomaly, Science, 324, 78–80, doi:10.1126/science.1166349, 2009.

Turner, J., Phillips, T., Hosking, J. S., Marshall, G. J., and Orr, A.: The Amundsen Sea low, Int. J. Climatol., 33, 1818–1829, doi:10.1002/joc.3558, 2013.

van Ommen, T. D. and Morgan, V.: Peroxide concentrations in the Dome summit south ice core, Law Dome, Antarctica, J. Geophys. Res-Atmos, 101, 15147–15152, doi:10.1029/96jd00838, 1996.

Vásquez Bedoya, L. F., Cohen, A. L., Oppo, D. W., and Blanchon, P.: Corals record persistent multidecadal SST variability in the Atlantic warm pool since 1775 AD, Paleoceanography, 27, PA3231, doi:10.1029/2012PA002313, 2012.

Villalba, R.: Climatic fluctuations in northern Patagonia during the last 1000 years as inferred from tree-ring records, Quaternary Res., 34, 346–360, doi:10.1016/0033-5894(90)90046-N, 1990.

Villalba, R., Boninsegna, J. A., Masiokas, M., Delgado, S., Aravena, J.-C., Roig, F. A., Schmelter, A., and Wolodarsky, A.: Large-scale temperature changes across the southern

CPD
11, 4159–4204, 2015

Andes: 20th-century variations in the context of the past 400 years, Climatic Change, 59, 177–232, 2003.
Villalba, R., Lara, A., Masiokas, M. H., Urrutia, R., Luckman, B. H., Marshall, G. J., Mundo, I. A., Christie, D. A., Cook, E. R., Neukom, R., Allen, K., Fenwick, P., Boninsegna, J. A., Srur, A. M., Morales, M. S., Araneo, D., Palmer, J. G., Cuq, E., Aravena, J. C., Holz, A., and LeQuesne, C.: Unusual Southern Hemisphere tree growth patterns induced by changes in the southern annular mode, Nat. Geosci., 5, 793–798, doi:10.1038/ngeo1613, 2012.
Vinther, B. M., Jones, P. D., Briffa, K. R., Clausen, H. B., Andersen, K. K., Dahl-Jensen, D., and Johnsen, S. J.: Climatic signals in multiple highly resolved stable isotope records from Greenland, Quaternary Sci. Rev., 29, 522–538, doi:10.1016/j.quascirev.2009.11.002, 2010.
Visbeck, M. and Hall, A.: Reply, J. Climate, 17, 2255–2258, doi:10.1175/1520-0442(2004)017<2255:R>2.0.CO;2, 2004.
von Gunten, L., Grosjean, M., Rein, B., Urrutia, R., and Appleby, P.: A quantitative high-resolution summer temperature reconstruction based on sedimentary pigments from Laguna Aculeo, central Chile, back to AD 850, Holocene, 19, 873–881, doi:10.1177/0959683609336573, 2009.
Wanamaker Jr, A. D., Kreutz, K. J., Schöne, B. R., Pettigrew, N., Borns, H. W., Introne, D. S., Belknap, D., Maasch, K. A., and Feindel, S.: Coupled North Atlantic slope water forcing on Gulf of Maine temperatures over the past millennium, Clim. Dynam., 31, 183–194, doi:10.1007/s00382-007-0344-8, 2007.
Widmann, M., Goosse, H., van der Schrier, G., Schnur, R., and Barkmeijer, J.: Using data assimilation to study extratropical Northern Hemisphere climate over the last millennium, Clim. Past, 6, 627–644, doi:10.5194/cp-6-627-2010, 2010.
Wiles, G. C., D'Arrigo, R. D., Barclay, D., Wilson, R. S., Jarvis, S. K., Vargo, L., and Frank, D.: Surface air temperature variability reconstructed with tree rings for the Gulf of Alaska over the past 1200 years, Holocene, 24, 198–208, doi:10.1177/0959683613516815, 2014.
Wilson, R., Miles, D., Loader, N. J., Melvin, T., Cunningham, L., Cooper, R., and Briffa, K.: A millennial long March–July precipitation reconstruction for southern-central England, Clim. Dynam., 40, 997–1017, doi:10.1007/s00382-012-1318-z, 2013.
Xiong, L. and Palmer, J. G.: Reconstruction of New Zealand temperatures back to AD 1720 using Libocedrus bidwillii tree-rings, Climatic Change, 45, 339–359, 2000.

CPD
11, 4159–4204, 2015

Yang, B., Qin, C., Wang, J., He, M., Melvin, T. M., Osborn, T. J., and Briffa, K. R.: A 3,500 year tree-ring record of annual precipitation on the northeastern Tibetan Plateau, P. Natl. A. Sci. USA, 111, 2903–2908, doi:10.1073/pnas.1319238111, 2014.

Yang, F., Wang, N., Shi, F., Ljungqvist, F. C., Wang, S., Fan, Z., and Lu, J.: Multi-proxy temperature reconstruction from the West Qinling Mountains, China, for the past 500 years, PLOS ONE, 8, e57638, doi:10.1371/journal.pone.0057638, 2013.

Yi, L., Yu, H., Ge, J., Lai, Z., Xu, X., Qin, L., and Peng, S.: Reconstructions of annual summer precipitation and temperature in north-central China since 1470 AD based on drought/flood index and tree-ring records, Climatic Change, 110, 469–498, doi:10.1007/s10584-011-0052-6, 2011.

Zinke, J., Dullo, W. C., Heiss, G. A., and Eisenhauer, A.: ENSO and Indian Ocean subtropical dipole variability is recorded in a coral record off southwest Madagascar for the period 1659 to 1995, Earth Planet. Sc. Lett., 228, 177–194, doi:10.1016/j.epsl.2004.09.028, 2004.

CPD
11, 4159–4204, 2015

Table A1. Proxy climate records used in PaleoR. Numbers in column 1 correspond to the locations plotted in Fig. 1.

No.	Region	Location	Proxy Data Type	Variable	[Lat, Lon]	References
1	Africa	Lake Verlorenvlei	Sediment diatom	Precipitation	[−33, 19]	Stager et al. (2012)
2	Africa	Lake Masoko	Sediment mag. susc.	Precipitation	[−9, 34]	Garcin et al. (2007)
3	Africa	Lake Malawi	Sediment TMAR	Precipitation	[−10, 34]	Johnson et al. (2001)
4	Africa	Makapansgat Valley	Speleothem lumin.	Temperature	[−24, 28]	Holmgren et al. (1999)
5	Africa	Makapansgat Valley	Speleothem δ^{18}O	Precipitation	[−24, 28]	Holmgren et al. (1999)
6	Africa	Makapansgat valley	Speleothem δ^{18}O	Temperature	[−24, 29]	Sundqvist et al. (2013)
7	Africa	Zimbabwe	Tree ring width	Precipitation	[−18, 29]	Therrell et al. (2006)
8	Africa	Morocco	Tree ring width	Precipitation	[33, 355]	Esper et al. (2007)
9	Indian Ocean	Mafia Island	Coral δ^{18}O	SST	[−8, 40]	Damassa et al. (2006)
10	Indian Ocean	Malindi	Coral δ^{18}O	SST	[−3, 40]	Cole et al. (2000)
11	Indian Ocean	Madagascar	Coral δ^{18}O	SST	[−24, 44]	Zinke et al. (2004)
12	Indian Ocean	Abrolhos	Coral δ^{18}O	SST	[−29, 113]	Kuhnert et al. (1999)
13	Indian Ocean	Salalah Arabia	Speleothem δ^{18}O	Precipitation	[18, 55]	Burns et al. (2002)
14	Indian Ocean	Flores Indonesia	Speleothem δ^{18}O	Precipitation	[−9, 121]	Griffiths et al. (2009)
15	Pacific	Guam Territory	Coral δ^{18}O	SST	[13, 145]	Asami et al. (2005)
16	Pacific	New Caledonia	Coral Sr/Ca	SST	[−22, 166]	Delong et al. (2012)
17	Pacific	Vanuatu	Coral δ^{18}O	SST	[−15, 167]	Quinn et al. (1993)
18	Pacific	Fiji and Tonga	Coral δ^{18}O	SLP	[−15, 180]	Linsley et al. (2008)
19	Pacific	Palmyra	Coral δ^{18}O	SST	[6, 198]	Cobb et al. (2003)
20	Pacific	Cook Is	Coral Growth	SST	[−22, 201]	Goodwin and Harvey (2008)
21	Pacific	Moorea	Coral δ^{18}O	SST	[−18, 210]	Boiseau et al. (1998)
22	Pacific	Secas Island	Coral δ^{18}O	Precipitation	[8, 278]	Linsley et al. (1994)
23	Pacific	El Junco Galapagos	Sediment grainsize	Precipitation	[−1, 271]	Conroy et al. (2008)
24	Pacific	Solomon Islands	Speleothem δ^{18}O	Precipitation	[−10, 160]	Maupin et al. (2014)
25	Pacific	Vanuatu	Speleothem δ^{18}O	Precipitation	[−18, 168]	Partin et al. (2013)
26	Pacific	NADA	Tree ring	Precipitation	[28, 255]	Cook et al. (2004)
27	Australia	Great Barrier Reef	Coral luminescence	Precipitation	[−18, 146]	Lough et al. (2011)
28	Australia	Great Barrier Reef	Coral Sr/Ca	SST	[−18, 146]	Hendy et al. (2002)
29	Australia	Great Barrier Reef	Coral luminescence	Precipitation	[−20, 147]	Hendy et al. (2003)
30	Australia	Lake Frome	Sediment shoreline	Precipitation	[−30, 139]	Cohen et al. (2011, 2012)
31	Australia	Lake Surprise	Sediment	Precipitation	[−38, 141]	Barr (2014)
32	Australia	Coastal N.S.W	Dune sediments	Wave Clim.	[−33, 151]	Goodwin et al. (2006)
33	Australia	Lake Tay	Tree ring width	Precipitation	[−33, 121]	Cullen and Grierson (2008)
34	Australia	Mt Read Tasmania	Tree ring width	Temperature	[−42, 145]	Cook et al. (2006)
35	New Zealand	Regional	Multiproxy	Precipitation	[−44, 168]	Lorry et al. (2008)
36	New Zealand	NZ South Island	Sediment moraine	Precipitation	[−44, 170]	Schaefer et al. (2009)
37	New Zealand	Oroko Swamp NZ	Tree ring width	Temperature	[−43, 170]	Cook et al. (2002)

CPD
11, 4159–4204, 2015

Table A1. Continued.

No.	Region	Location	Proxy Data Type	Variable	[Lat, Lon]	References
38	New Zealand	NZ North Island	Tree ring width	SLP	[−37, 175]	Fowler et al. (2008)
39	New Zealand	Mangawhero NZ	Tree ring width	Temperature	[−39, 176]	D'Arrigo et al. (1998, 2000)
40	New Zealand	Takapari NZ	Tree ring width	Temperature	[−40, 176]	Xiong and Palmer (2000)
41	South America	Quelccaya, Peru	Ice accumulation	Precipitation	[−14, 289]	Thompson (1992)
42	South America	Quelccaya, Peru	Ice core $\delta^{18}O$	Temperature	[−14, 289]	Thompson et al. (2006)
43	South America	South Patagonia	Multiproxy	Precipitation	[−50, 287]	Neukom et al. (2010)
44	South America	South Patagonia	Multiproxy	Temperature	[−50, 287]	Neukom et al. (2010)
45	South America	Central Chile	Multiproxy	Precipitation	[−32, 290]	Neukom et al. (2010)
46	South America	Central Chile	Multiproxy	Temperature	[−32, 290]	Neukom et al. (2010)
47	South America	Subtropics	Multiproxy	Precipitation	[−25, 290]	Neukom et al. (2010)
48	South America	Subtropics	Multiproxy	Temperature	[−25, 290]	Neukom et al. (2010)
49	South America	Lago Guanaco	Sediment carbonate	Precipitation	[−52, 287]	Moy et al. (2008)
50	South America	Laguna Aculeo	Sediment pigments	Temperature	[−34, 288]	von Gunten et al. (2009)
51	South America	Patagonian Andes	Sediment laminae	Precipitation	[−47, 289]	Elbert et al. (2011)
52	South America	South Orkney Is	Sediment $\delta^{18}O$	Temperature	[−61, 315]	Noon et al. (2003)
53	South America	South Georgia Is	Sediment moraine	Temperature	[−54, 324]	Clapperton (1990)
54	South America	North Andes	Tree ring width	Temperature	[−41, 288]	Villalba et al. (2003)
55	South America	Chilean Cordillera	Tree ring width	Precipitation	[−33, 288]	LeQuesne et al. (2006)
56	South America	Rio Alerce	Tree ring width	Temperature	[−41, 289]	Villalba (1990)
57	South America	Patagonia	Tree ring width	Precipitation	[−41, 289]	Villalba (1990)
58	South America	Andes	Tree ring width	Precipitation	[−37, 290]	Christie et al. (2009)
59	Antarctica	Droning Maude Land	Ice core $\delta^{18}O$	Temperature	[−75, 1]	Oerter et al. (2011)
60	Antarctica	Law Dome	Ice core $\delta^{18}O$	SLP	[−66, 112]	Van Ommen et al. (1997)
61	Antarctica	Law Dome	Ice core Na^{+}	SLP	[−66, 112]	Goodwin et al. (2004)
62	Antarctica	Vic. Lower Glacier	Ice core δD	Temperature	[−77, 167]	Bertler et al. (2011)
63	Antarctica	Vic. Lower Glacier	Ice core Fe^{+}	SLP	[−77, 167]	Bertler et al. (2011)
64	Antarctica	Vic. Lower Glacier	Ice core Na^{+}	SLP	[−77, 167]	Bertler et al. (2011)
65	Antarctica	Mt. Erebus	Ice core δD	Temperature	[−78, 168]	Rhodes et al. (2012)
66	Antarctica	Siple Dome	Ice core Na +	SLP	[−81, 212]	Kreutz and Mawyeski (2000)
67	Antarctica	West Antarctic	Ice accumulation	Precipitation	[−79, 248]	Banta et al. (2008)
68	Antarctica	James Ross Island	Ice core δD	Temperature	[−64, 302]	Abram et al. (2013)
69	Antarctica	James Ross Island	Ice core melt	Temperature	[−64, 302]	Abram et al. (2013)
70	Europe	Europe Alps	Documentary	Temperature	[47, 7]	Casty et al. (2005)
71	Europe	Europe Alps	Documentary	Temperature	[47, 7]	Casty et al. (2005)
72	Europe	Europe Alps	Documentary	Precipitation	[47, 7]	Casty et al. (2005)
73	Europe	Europe Alps	Documentary	Precipitation	[47, 7]	Casty et al. (2005)
74	Europe	Scotland	Speleothem growth	Precipitation	[58, 356]	Proctor et al. (2002)
75	Europe	Iberia	Speleothem $\delta^{13}C$	Temperature	[43, 356]	Martìn-Chivelet et al. (2011)
76	Europe	Central Europe	Tree ring width	Temperature	[50, 9]	Büntgen et al. (2010)
77	Europe	Central Europe	Tree ring width	Precipitation	[50, 9]	Büntgen et al. (2010)
78	Europe	Europe Alps	Tree multiproxy	Temperature	[46, 10]	Trachsel et al. (2012)
79	Europe	Jämtland	Tree MXD	Temperature	[62, 14]	Gunnarson et al. (2011)

CPD
11, 4159–4204, 2015

Table A1. Continued.

No.	Region	Location	Proxy Data Type	Variable	[Lat, Lon]	References
80	Europe	Scandinavia	Tree MXD	Temperature	[68, 20]	Esper et al. (2014)
81	Europe	Tatra Mountains	Tree ring width	Temperature	[50, 20]	Büntgen et al. (2013)
82	Europe	Finland	Tree MXD	Temperature	[62, 28]	Helama et al. (2014)
83	Europe	Aegean	Tree ring width	Precipitation	[41, 29]	Griggs et al. (2007)
84	Europe	Central England	Tree ring width	Precipitation	[52, 359]	Wilson et al. (2013)
85	Atlantic	Yucatan	Coral growth rates	SST	[21, 273]	Vasquez et al. (2012)
86	Atlantic	Tortuga	Coral Sr/Ca	SST	[25, 277]	DeLong et al. (2014)
87	Atlantic	Bahamas	Coral growth rates	SST	[26, 281]	Saenger et al. (2009)
88	Atlantic	Chesapeake Bay	Coral Mg/Ca	SST	[37, 284]	Cronin et al. (2003)
89	Atlantic	Puerto Rico	Coral Sr/Ca	SST	[18, 293]	Kilbourne et al. (2008)
90	Atlantic	Bermuda	Coral Sr/Ca	SST	[32, 296]	Goodkin et al. (2008)
91	Atlantic	Nordic Sea	Sediment ocean	SST	[67, 8]	Cunningham et al. (2013)
92	Atlantic	Gulf of Maine	Sediment δ^{18}O	SST	[44, 292]	Wanamaker et al. (2007)
93	Atlantic	Caraico Basin	Sediment Mg/Ca	SST	[11, 295]	Black et al. (2007)
94	Atlantic	Iceland Shelf	Sediment ocean	SST	[67, 342]	Cunningham et al. (2013)
95	North America	Washington	Sediment lake δ^{18}O	Precipitation	[49, 242]	Steinman et al. (2012)
96	North America	Baffin Island	Sediment varves	Temperature	[60, 293]	Thomas et al. (2009)
97	North America	Firth River Alaska	Tree MXD	Temperature	[69, 218]	Anchukaitis et al. (2013)
98	North America	Gulf of Alaska	Tree ring	Temperature	[59, 220]	Wiles et al. (2014)
99	North America	Oregon	Tree ring width	Precipitation	[42, 238]	Malevich et al. (2013)
100	North America	California	Tree ring δ^{13}C	Precipitation	[37, 242]	Bale et al. (2011)
101	North America	Canadian Rockies	Tree MXD	Temperature	[52, 243]	Luckman et al. (2005)
102	North America	Great Basin	Tree ring width	Temperature	[38, 244]	Salzer et al. (2013)
103	North America	Colorado	Tree ring width	Temperature	[35, 248]	Salzer et al. (2005)
104	North America	Colorado Basin	Tree ring width	Precipitation	[39, 252]	Meko et al. (2007)
105	North America	Barranca	Tree ring	Precipitation	[19, 261]	Stahle et al. (2011)
106	North America	Colorado	Tree ring width	Precipitation	[30, 262]	Cleaveland et al. (2011)
107	North America	West Virginia	Tree ring width	Precipitation	[39, 281]	Maxwell et al. (2012)
108	North America	Potomac River	Tree ring width	Precipitation	[39, 284]	Maxwell et al. (2011)
109	North America	New York City	Tree ring	Precipitation	[41, 286]	Pederson et al. (2013)
110	North America	Eastern Canada	Tree ring	Temperature	[54, 288]	Gennaretti et al. (2014)
111	Arctic	Agassiz Ice Cap	Ice core δ^{18}O	Temperature	[81, 287]	Fisher et al. (1995)
112	Arctic	DYE-3 Greenland	Ice core δ^{18}O	Temperature	[65, 316]	Vinther et al. (2010)
113	Arctic	GRIP Greenland	Ice core δ^{18}O	Temperature	[73, 322]	Vinther et al. (2010)
114	Arctic	Greenland	Ice core δ^{18}O	Temperature	[73, 323]	Kobashi et al. (2011)
115	Arctic	Crete Greenland	Ice core δ^{18}O	Temperature	[71, 323]	Vinther et al. (2010)
116	Asia	North China	Documentary	Precipitation	[37, 111]	Yi et al. (2011)
117	Asia	North China	Documentary	Temperature	[37, 111]	Yi et al. (2011)
118	Asia	Altai	Ice core δ^{18}O	Temperature	[50, 87]	Eichler et al. (2009)
119	Asia	China	Speleothem	Precipitation	[37, 111]	Tan et al. (2011)
120	Asia	Beijing	Speleothem layer	Temperature	[40, 116]	Tan et al. (2003)
121	Asia	Yamalia	Tree ring width	Temperature	[67, 68]	Briffa et al. (2013)

CPD
11, 4159–4204, 2015

Table A1. Continued.

No.	Region	Location	Proxy Data Type	Variable	[Lat, Lon]	References
122	Asia	Kathmandu	Tree ring width	Temperature	[28, 84]	Cook et al. (2003)
123	Asia	Kathmandu	Tree ring width	Temperature	[28, 84]	Cook et al. (2003)
124	Asia	Tibet	Tree ring width	Precipitation	[38, 99]	Yang et al. (2014)
125	Asia	Selenge River	Tree ring width	Precipitation	[49, 100]	Davi et al. (2006)
126	Asia	Qinling Mountains	Tree ring multiproxy	Temperature	[34, 104]	Yang et al. (2013)
127	Asia	North-central China	Tree MXD	Temperature	[34, 106]	Chen et al. (2014)
128	Asia	Yeruu River	Tree ring width	Precipitation	[50, 107]	Pederson et al. (2013)
129	Asia	Kherlen River	Tree ring width	Precipitation	[47, 111]	Davi et al. (2013)
130	Asia	Hokkaido	Tree MXD	Temperature	[44, 143]	Davi et al. (2002)

CPD
11, 4159–4204, 2015

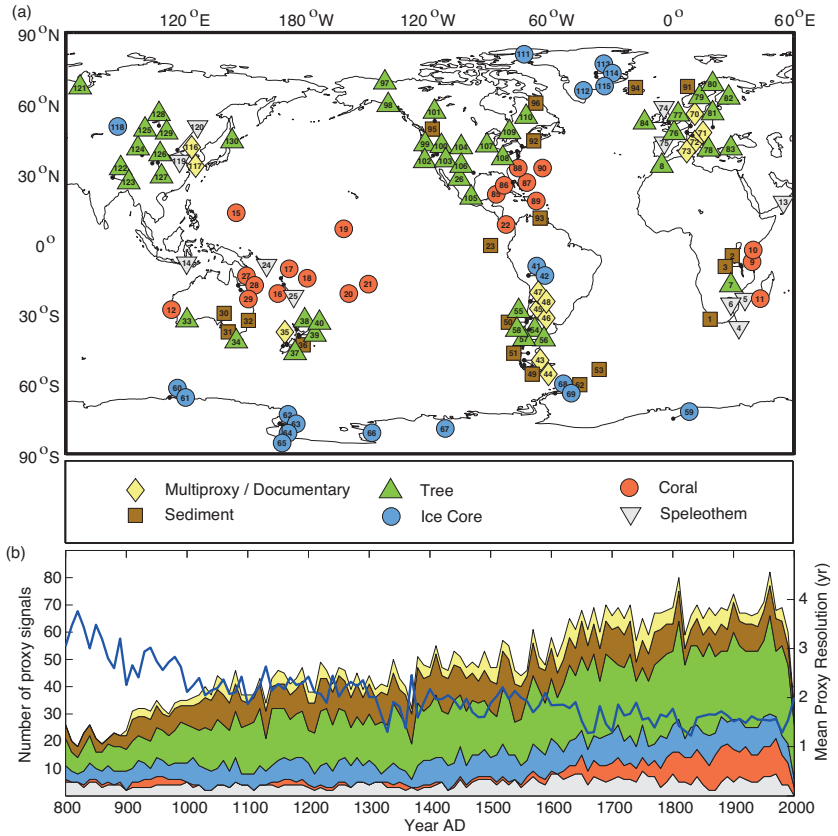

Figure 1. (a) Proxy map showing locations and types of proxy data included in PaleoR; numbers correspond to individual records listed in Table A1. **(b)** Density (number of individual records) of proxy data used at each timestep; blue line represents the mean temporal resolution of all proxy records at each timestep.

CPD
11, 4159–4204, 2015

The Paleoclimate reanalysis project

S. A. Browning and I. D. Goodwin

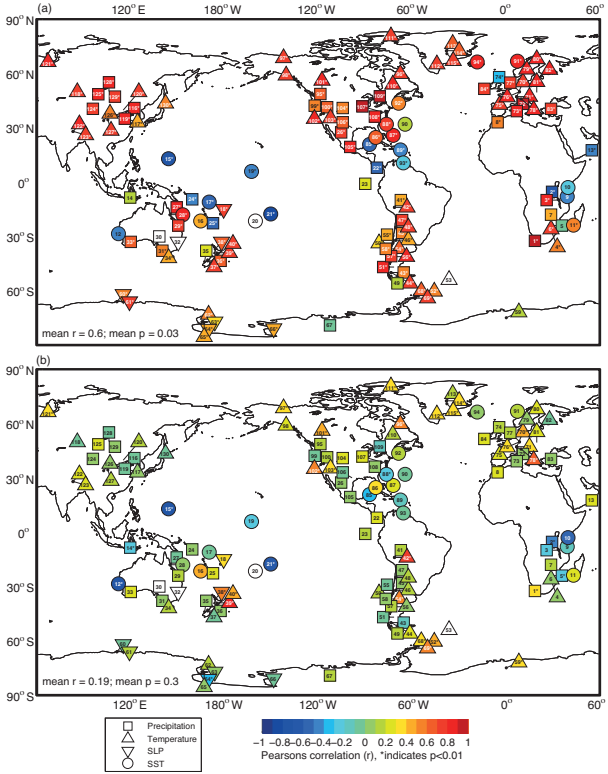

Figure 2. Correlations (Pearson's *r*) between each proxy record and the equivalent climate variable derived from **(a)** PaleoR and **(b)** LME ensemble mean; numbers correspond to individual records listed in Table A1. Correlations are calculated using decadal means, * denotes significant correlations ($p < 0.01$). Significant negative correlations typically denote proxies that have an inverse relationship to their respective climatic variables. Mean correlation values are based on the absolute *r* values.

CPD
11, 4159–4204, 2015

The Paleoclimate reanalysis project

S. A. Browning and I. D. Goodwin

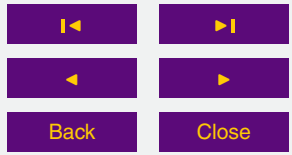

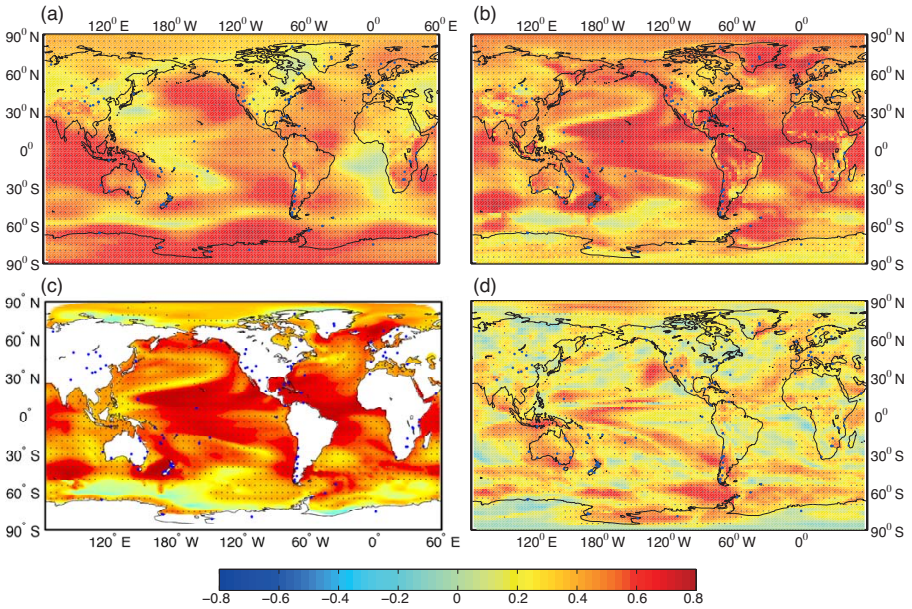

Figure 3. Pseudoproxy experiment results: grid point correlations (Pearson's r) between LME^{01} and PaleoR^{pseudoproxy} calculated at decadal resolution over the over 850–2000 AD period for **(a)** SLP, **(b)** air temperature, **(c)** SST, and **(d)** precipitation. Blue dots illustrate the spatial distribution of pseudoproxy data. Stippling indicates statistically significant correlations ($p < 0.01$).

CPD
11, 4159–4204, 2015

The Paleoclimate reanalysis project

S. A. Browning and I. D. Goodwin

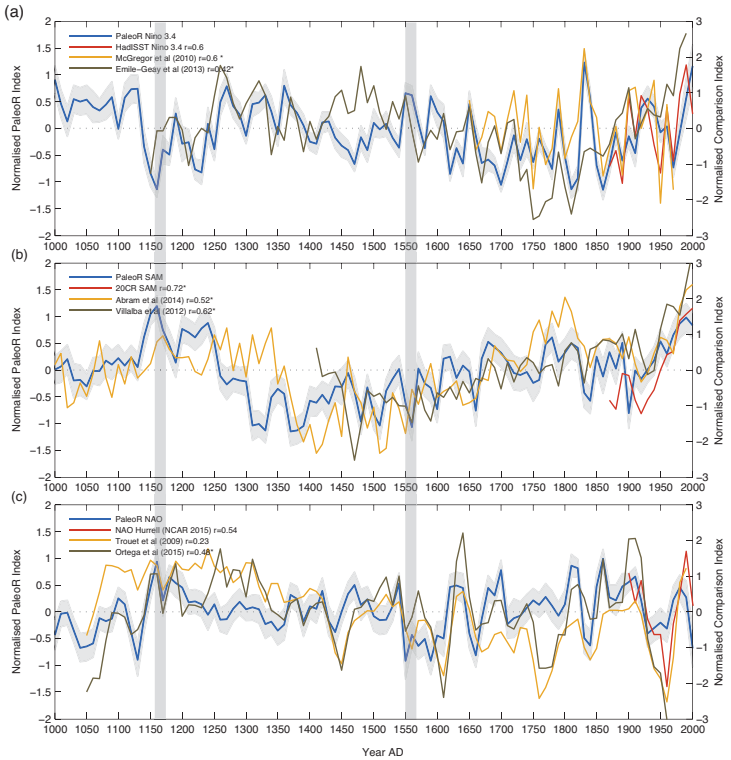

Figure 4. Timeseries plots showing three PaleoR derived reconstructions of major modes of global climate variability: **(a)** ENSO, **(b)** SAM, and **(c)** NAO. Shading on PaleoR timeseries defines the 95 % confidence interval of the 50-member BMA ensemble mean at each timestep. Plotted for comparison are equivalent indices derived from both proxy and observational data; * denotes statistically significant correlations ($p < 0.01$). Vertical bars indicate time period used for spatial plots in Fig. 5.

CPD
11, 4159–4204, 2015

The Paleoclimate reanalysis project

S. A. Browning and I. D. Goodwin

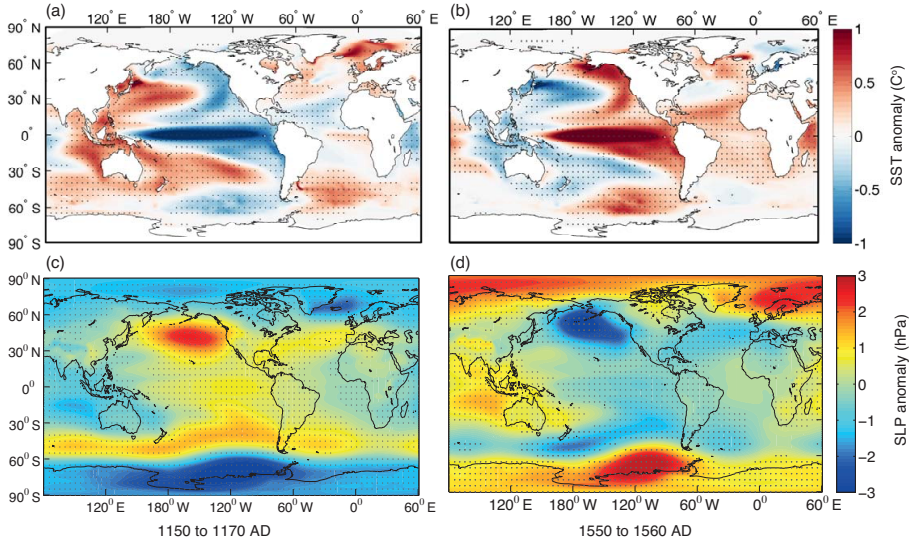

Figure 5. PaleoR derived **(a–b)** SST and **(c–d)** SLP anomaly spatial fields for two time periods, **(a–c)** 1150–1170 AD and **(b–d)** 1550–1560 AD, selected to highlight positive and negative phases of each index, as identified in Fig. 4. During 1150–1170 AD (1550–1560 AD) generally negative (positive) Nino3.4 SST were coupled to a positive (negative) SAM and NAO (Fig. 4). Each gridded field is a composite of the 50-member BMA ensemble each timestep; stippling indicates statistically significant anomalies ($p < 0.01$).

CPD
11, 4159–4204, 2015